Investigating fluid exchange between granitic hosts, dykes and enclaves in the South Mountain Batholith

Dana Thomsen

SUBMITTED IN PARTIAL FULFILLMENT OF THE REQUIREMENTS FOR THE
UNDERGRADUATE RESEARCH THESIS
DEPARTMENT OF EARTH SCIENCES
DALHOUSIE UNIVERSITY, HALIFAX, NOVA SCOTIA

April 2018

Distribution License

DalSpace requires agreement to this non-exclusive distribution license before your item can appear on DalSpace.

NON-EXCLUSIVE DISTRIBUTION LICENSE

You (the author(s) or copyright owner) grant to Dalhousie University the non-exclusive right to reproduce and distribute your submission worldwide in any medium.

You agree that Dalhousie University may, without changing the content, reformat the submission for the purpose of preservation.

You also agree that Dalhousie University may keep more than one copy of this submission for purposes of security, back-up and preservation.

You agree that the submission is your original work, and that you have the right to grant the rights contained in this license. You also agree that your submission does not, to the best of your knowledge, infringe upon anyone's copyright.

If the submission contains material for which you do not hold copyright, you agree that you have obtained the unrestricted permission of the copyright owner to grant Dalhousie University the rights required by this license, and that such third-party owned material is clearly identified and acknowledged within the text or content of the submission.

If the submission is based upon work that has been sponsored or supported by an agency or organization other than Dalhousie University, you assert that you have fulfilled any right of review or other obligations required by such contract or agreement.

Dalhousie University will clearly identify your name(s) as the author(s) or owner(s) of the submission, and will not make any alteration to the content of the files that you have submitted.

If you have questions regarding this license please contact the repository manager at dalspace@dal.ca.

Grant the distribution license by signing and dating below.

_____   _____

Name of signatory   Date

DALHOUSIE UNIVERSITY

Department of Earth Sciences
Halifax, Nova Scotia
Canada B3H 4R2
(902) 494-2358

DATE: March 30th, 2018

AUTHOR: Dana Thomsen

TITLE: Investigating fluid exchange between granitic hosts, dykes and enclaves in the South Mountain Batholith

DEGREE: BSc Earth Sciences   CONVOCATION: June   YEAR: 2018

Permission is herewith granted to Dalhousie University to circulate and to have copied for non-commercial purposes, at its discretion, the above title upon the request of individuals or institutions.

_____
Signature of Author

Abstract

This study performed detailed geochemical analyses of primary and secondary minerals from the Sambro Head dyke in order to further investigate the hypothesis that it was formed via hybridization. Recent studies have suggested that mafic enclaves within the (Late Devonian) South Mountain Batholith are mela-granitic restites formed in part from the melting of metasedimentary rocks. Detailed textural studies conducted in the Sambro Head area have revealed clear evidence of magma mixing between the host granite and a mafic dyke intrusion. Textural and micro-analytical studies also show resorption textures and Ba zoning in K-Feldspar megacrysts, indicating significant temperature changes, supporting the hypothesis that hybridization has occurred. However, hybridization and fluid-alteration of the dyke makes determining the original composition extremely difficult. This study investigated the fluid exchange reactions between the host granitic rock and the Sambro Head dyke using whole rock relationships as well as the analysis of fluid-bearing phases. Whole rock samples from the dyke, the mixing zone, and the adjacent peraluminous granites were collected and analyzed using the Electron Probe Micro-Analyzer (EPMA) and Laser Ablation Inductively Coupled Plasma Mass Spectrometry (LA-ICP-MS). The dyke's mineral assemblage consists of plagioclase + quartz + biotite + oxides, along with secondary chlorite + muscovite and a significant amount of apatite, much of which appears to be primary. The extensive chlorite + muscovite replacement of biotite indicates continued fluid exchange reactions prior to final crystallization of the dyke. EPMA maps and thin section data show that this replacement is fairly consistent in all samples from within the dyke, with slightly higher replacement of biotite occurring near the edges of the dyke. The biotite selvage adjacent to the mixing zone also suggests evidence of disequilibrium and fluid exchange between the dyke and the granitic host. Small groups of cordierite can be found in similar places, along the edge of the dyke. Three geothermometry methods: Titanium-in-biotite, biotite-apatite and chlorite geothermometry were applied to calculate mineral formation temperatures of the dyke. Peak formation temperatures using the Titanium-in-biotite and biotite apatite methods were ~648°C and ~542°C respectively. The resulting chlorite peak formation temperature was ~325°C. These were used to create a temperature profile and crystallization history of the Sambro Head dyke supporting the hypothesis that hybridization occurred.

Keywords: dyke, hybridization, fluid reactions, magma mixing, geothermometry

Table of Contents

Table of Figures

List of Tables

Table of Mineral Abbreviations

Mineral Name	Mineral Abbreviation
Quartz	Qtz
Biotite	Bt
K-feldspar	Kfs
Plagioclase	Pl
Muscovite	Ms
Chlorite	Chl
Ilmenite	Ilm
Titanite	Ttn
Sericite	Ser
Apatite	Ap
Magnetite	Mag

Mineral abbreviations from Kretz (1983)

Acknowledgements

I would like to extend my greatest thanks to my supervisor Dr. Richard Cox. You challenged me to produce science that was thorough and that I am proud of. Your unwavering support and encouraging words will not be forgotten.

Thanks, must also be made out to Dan MacDonald from the Robert M. MacKay Microprobe Laboratory. Many hours were spent collecting EPMA data and would not have gone so smoothly if it were not for your guidance.

Additional thanks to Dr. James Brenan and those in his research group (Dalhousie Laboratory for Experimental High Pressure Geological Research), for the use and help with the high-temperature furnace and LA-ICP-MS.

Thanks, to my close friends and family for editing many, many drafts of my thesis and for being great throughout this whole experience.

Finally, I would like to thank the 2017/2018 honours class. There were many great laughs and struggles throughout this year but in the end we did it!

Chapter 1: Introduction

1.1 Opening Statement

This study seeks to investigate the fluid-bearing phases of the Sambro Head dyke section from Bald Rock, Nova Scotia. Its focus is to determine the crystallization history of the dyke, by examining the thermal profile reordered by the main fluid-bearing minerals and by examining whole-rock major and trace-element compositions. Previous studies from this area have discovered evidence of magma mixing and various mineral textures, supporting the hypothesis that some hybridization has occurred in the Halifax Pluton (Wongus, 2013 and Stashin, 2017). Hybridization is a process where two partially molten melts interact and evolve (Westerman et al., 2004). The evolution of this mixed magma alters the original composition drastically and involves detailed textural and geochemical analysis in order to be confirmed. Due to the extensive fluid-exchange that occurred during and after emplacement, the Sambro Head dyke and adjacent enclaves are now represented by a mineral assemblage which recorded multiple cooling processes. Understanding these fluid-exchange reactions, by analyzing the fluid-bearing phases, thus becomes critical in order to reveal the petrogenesis of the dyke. An emphasis was made on investigating the mica and chlorite fluid-bearing phases, and this data was used to suggest a petrochemical classification for the dyke.

1.2 Objectives

The aim of this study was to complete geochemical analyses on the Sambro Head dyke, more specifically, looking into the fluid-bearing phases (micas and chlorite), to determine the original composition of the dyke. This was done using existing field observations and textural examinations (Wongus, 2013 and Stashin, 2017), conducting whole rock chemical analysis and the micro-analysis of biotite, muscovite and chlorite. These investigations were completed using the following approach:

(1) Prepared existing samples from Sambro Head dyke (Stashin, 2017), by further grinding the rock into a very fine powder

(2) Completed lab work by fusing whole rock powder into glasses for Electron Probe Micro-Analyzer (EPMA) analysis. Conducted micro-analysis, using EPMA, of the micas, chlorite, and apatite from the existing thin sections.

(3) Laser Ablation Induced Coupled Plasma Mass Spectrometry (LA-ICP-MS) work was also done on both whole rock glasses and thin sections to acquire trace-element and isotopic data.

(4) Used geothermometry to examine fluid/rock temperature profiles recorded, allowing a more complete crystallization history to be determined.

1.3 Geologic Setting

The South Mountain Batholith (SMB) is a Late Devonian, ca. 370 Ma, intrusive igneous body that covers most of the southwestern portion of the province of Nova Scotia, Canada. It intrudes the Meguma Terrane, laying to the south of the Cobequid-Chedabucto Fault Zone. The South Mountain Batholith overlies the Silurian to Early Devonian, Rockville Notch Group, as well as the Cambrian to Early Ordovician Halifax and Goldenville groups (Figure 1).
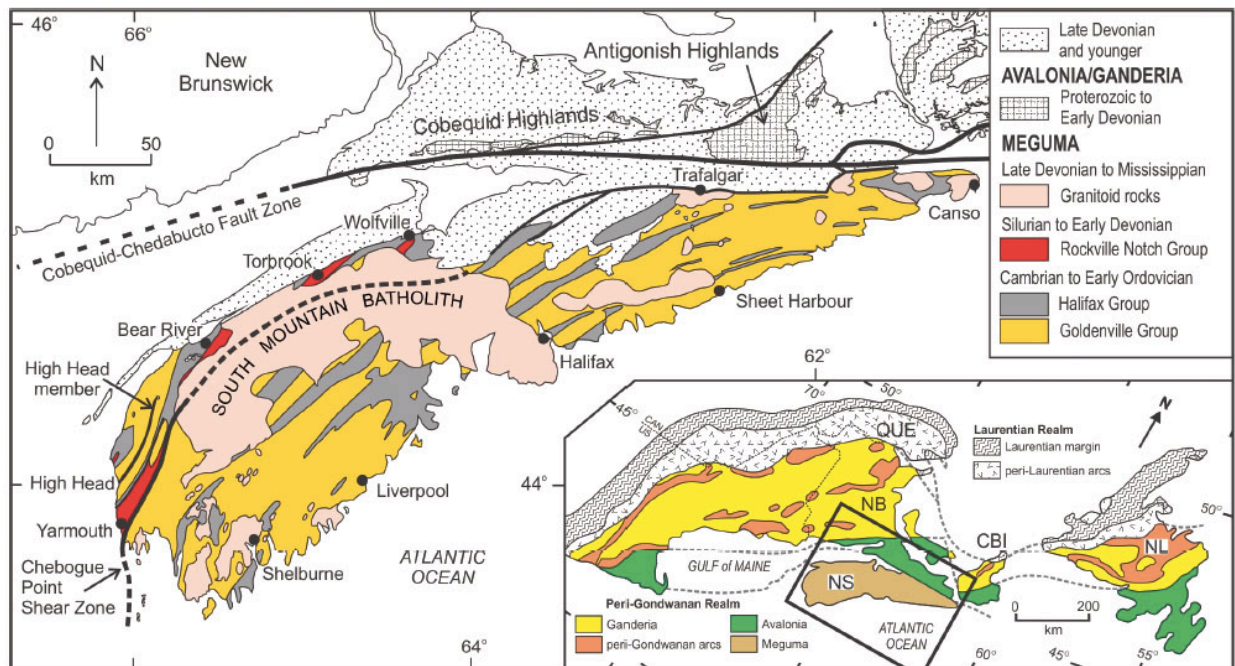
Figure 1 - Map of the Geology of Nova Scotia taken from White and Barr (2012)

The SMB is composed of post-tectonic peraluminous granitoids that contains thirteen distinguishable plutons. These plutons have been sub-divided into stages which classify their emplacement and varying compositions: stage one contains five of the thirteen plutons, and stage two contains the remaining eight plutons (Horne et al., 1992). The focus of this study will be on the Halifax Pluton, a predominantly biotite monzogranite complex, from stage two (Figure 2). This biotite monzogranite is known to contain features indicating a transpression during emplacement, represented by the presence of mineral alignment, xenocrysts and megacrysts, enclaves and dykes (Horne et al., 1992).
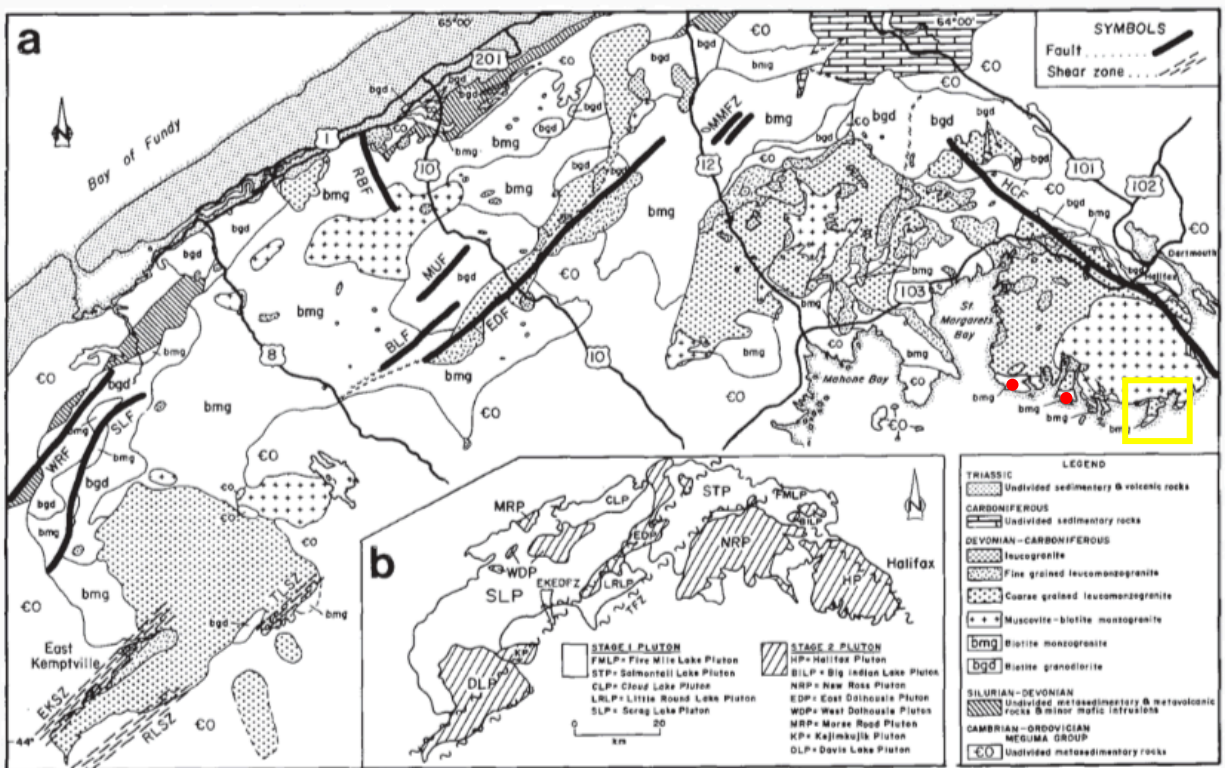
Figure 2 - Map of the South Mountain Batholith plutons from Horne et al. (1992) – Sambro Head outlined in yellow box Prospect and Peggy's Cove noted by red dots

1.3.1 Sampling Area

This study focused on the dyke in Sambro Head, Nova Scotia. Sambro Head is located between St. Margaret's Bay and Halifax Harbour, along the shore of Bald Rock (Figure 2). The dyke's orientation is roughly north-south with its exposure extending for one hundred metres, from the cliff face toward the Atlantic Ocean. Sampling and field observations were conducted by Sydney Stashin and Dr. Richard Cox in the fall of 2016 (Stashin, 2017). A total of seven

samples were collected from a north-facing outcrop of the Sambro Head dyke. The samples were strategically taken from the following sections of the dyke; the host granite, mixing zone between the dyke and granite, and various interior sections of the dyke (Figure 3). Samples 2, 6, and 7 were taken from the edges of the dyke (close but not part of the mixing zone), and samples 1 and 5 taken from more central locations within the dyke. Sample 4 was collected from the mixing zone, and sample 3 was taken from the adjacent granite. Field observations and corresponding photos show that this dyke is heterogeneous and has experienced significant magma mixing with the host granite upon emplacement. Figure 4 illustrates the irregular boundaries of the dyke and the extensive magma mingling textures. Additional granite samples from Prospect and Peggy's Cove, Nova Scotia (Figure 2) were used for comparison and were collected by Derek Wongus in 2013.

Figure 3 - Photo of the sampling area and of all samples collected – modified from Stashin (2017)
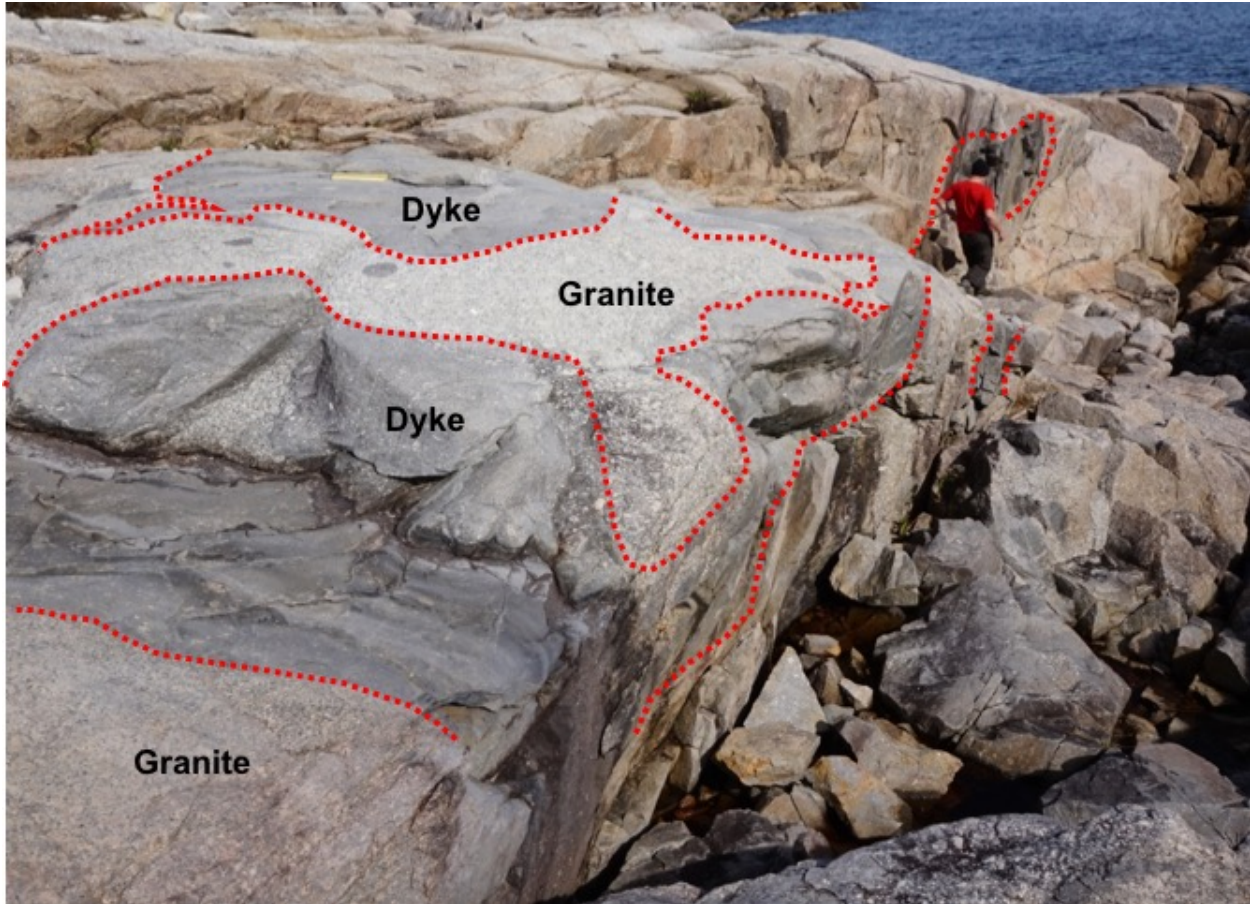
Figure 4 - Photo of entire exposed dyke section - dyke outlined to highlight irregular boundaries – modified from Stashin (2017)

1.4 Previous Evidence to Support Hybridization

Investigations have been ongoing across the biotite-monzogranite zone of the South Mountain Batholith for more than twenty years. Recent studies conducted by Wongus in 2013 and Stashin in 2017, examined the micro-textural evidence for magma mixing and hybridization in the Peggy's Cove, Prospect and Sambro Head regions. The granites from these regions contain large numbers of K-feldspar megacrysts, with oscillatory zoning present in the cores (Figure 5) (Wongus, 2013 and Stashin, 2017). The Sambro Head dyke section also contains K-feldspar megacrysts. Oscillatory zoning patterns within the megacrysts can be seen in both the granite and the dyke. However, the K-feldspars of the dyke section were shown to be resorbed, indicating that they were not in equilibrium with the mafic melt during emplacement and that these feldspars were inherited from the host granitic magma (Stashin, 2017). Changes in barium levels across the K-feldspar crystals were detected in various parts of the Sambro Head dyke. Data

from a line scan of the crystal (path of the line scan is denoted by the red line in Figure 6), shows a steady decrease in barium from the edge of the megacryst to about 200 μm into the centre (Figure 6). The weight percent of barium then increases at a distance of 280 μm by roughly 0.18 percent (Figure 6). These cycles are attributed to the resorption process and suggest that significant temperature changes occurred during megacrysts growth in these magmas (Stashin, 2017).

Figure 5 - Photos of the K-feldspar megacrysts from the Sambro Head region – megacrysts in dyke (on left) and in adjacent granite (on right) – modified from Stashin (2017)
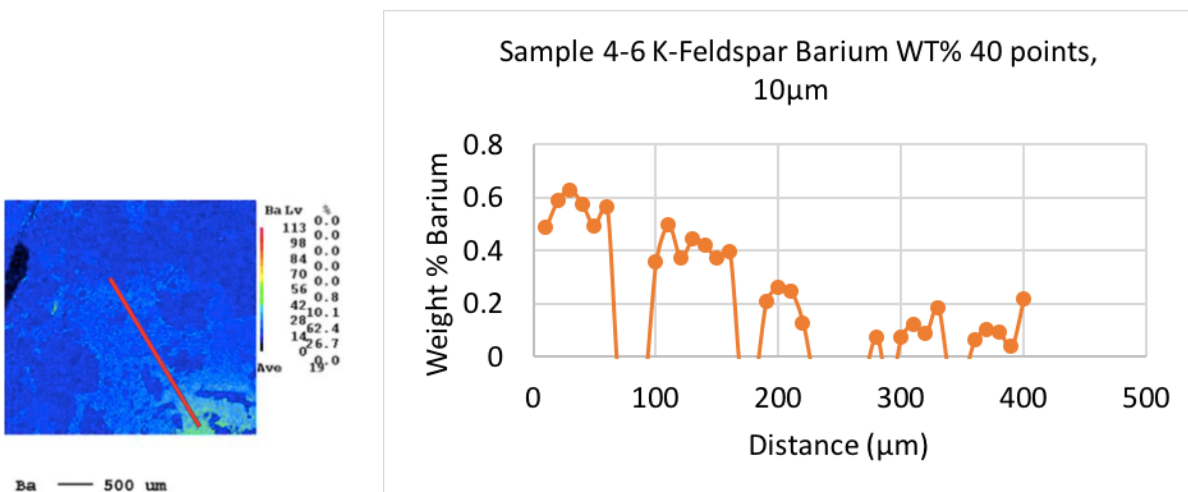
Figure 6 - X-Ray map of Ba zoning in K-feldspar crystal and line graph of the trends in Ba across the crystal from Stashin (2017)

A study done on the Shap Granite in Northern England by Cox et al. (1996), yielded very similar results to the above investigations by Wongus (2013) and Stashin (2017). K-feldspars in the Shap Granite also showed oscillatory zoning and cyclical changes of barium. Cox et al. (1996), suggested that this was linked to the emplacement of several intrusions of basic magmas, mixing in with the granite, causing the hybridization.

1.4.1 Alternative Hypotheses to Hybridization

A recent paper published by MacDonald and Clarke (2017), has hypothesized that enclaves found in the Sambro Head region are melagranitic restites, formed in part by the melting and contamination of the adjacent Meguma Supergroup metasediments. The interpretations from this study claim that the field relationships, mineralogical data, textural features, and chemical composition make the enclaves the products of portions of the South Mountain Batholith that did not fully assimilate. The lack of the dispersal of material has left regions of the Batholith with more concentrated, varying compositions (MacDonald and Clarke, 2017). The Sambro Head dyke, which is of a similar composition to the previously mentioned mafic enclaves (Wongus, 2013), is also referenced and named as a Late Devonian mafic intrusion (LDMI). Macdonald and Clarke (2017), deem the enclaves found adjacent to the Sambro Head dyke and in the nearby regions to be independent from the mafic intrusion event. It is not clear, however, that the objects being described as melagranites and enclaves in the SMB are the same object. Considerable textural variations have been described with regards to these mafic fragments (MacDonald and Clarke, 2017). The mafic dyke at Sambro Head, however, remains as the best example of an inter-magmatic intrusion within the SMB so far discovered.

Chapter 2: Analytical Methods

2.1 Whole Rock Analysis

Whole rock analyses are important to determine the conditions of formation and original compositions of igneous rocks. Detailed chemical analyses of the whole rock samples from the Sambro Head dyke were carried out to identify major and trace elements. Each of the seven samples collected from the Sambro Head dyke were cut in two pieces. One half of each of the samples was kept for creating thin sections. The other half of the samples was cut into three "bread like" slices, separating the upper, middle and lower sections. This separation technique was done to a) make the rock crushing process more manageable, and b) allow any geochemical variations within samples to be detectable, especially for mixing zone samples (3 and 4) which contained both granite and dyke materials (Figure 3). A total of twelve slices of the seven samples collected were crushed to create individual homogeneous powders (Stashin, 2017), and further refined using a mortar and pestle to produce very fine powders. The powders were then prepped to be fused into small glass beads, for later use in the EPMA and LA-ICP-MS.

2.1.1 Fusion of Whole Rock Powders

The whole rock powder fusion process produces small glass beads that can be mounted in epoxy, polished, and used for EPMA and LA-ICP-MS analysis. The fusion technique used for this study was flux-free. Advantages to using a flux-free fusion method are its convenience in creating whole rock glass beads with lower risk of contamination. The fusion process began with the production of graphite capsules to hold the whole rock powders. Graphite rods, 12 mm in diameter, were shallowly hollowed out using a standard lathe and cut to size using a jewlers saw (Figure 7). Graphite rods were selected because of their stability, being easy to cut and configure into solid containment capsules, and because they were readily accessible for use in this study. Whole rock powders were measured using a scientific scale and 40 mg of each powder was placed into an individual graphite capsule. Batches of four capsules were put into an alumina crucible and placed into a Lindberg-Blue high-temperature furnace (Figure 8). The alumina crucibles allowed for the easy placement and extraction of the samples from the furnace. Each batch of capsules was fused at 1500°C for 50 minutes. Once extracted, the samples were left to quench at room temperature (22°C). Three separate courses of fusions were conducted at

different temperatures, durations and quenches, to ensure that loss of volatiles and potential mineral growth was minimized.

Two preliminary fusions were completed prior to determining optimal conditions. The first fusion was conducted at 1400°C for 15 min with a room temperature quench, while the second fusion was conducted at 1400°C for 20 min with a water quench. Both of the early attempts produced unsatisfactory results with a lack of thorough melting and extensive fracturing from the water quenched samples limiting the surface area available for analysis. Optimal conditions were found to be those mentioned above, 1500°C for 50 min with a room temperature quench (22°C). Final steps following the fusion process included mounting the glass beads into epoxy disks. Standard epoxy was used to set the glasses, followed by a 4-step, two stage fine sandpaper and two stage alumina paste polishing procedure.
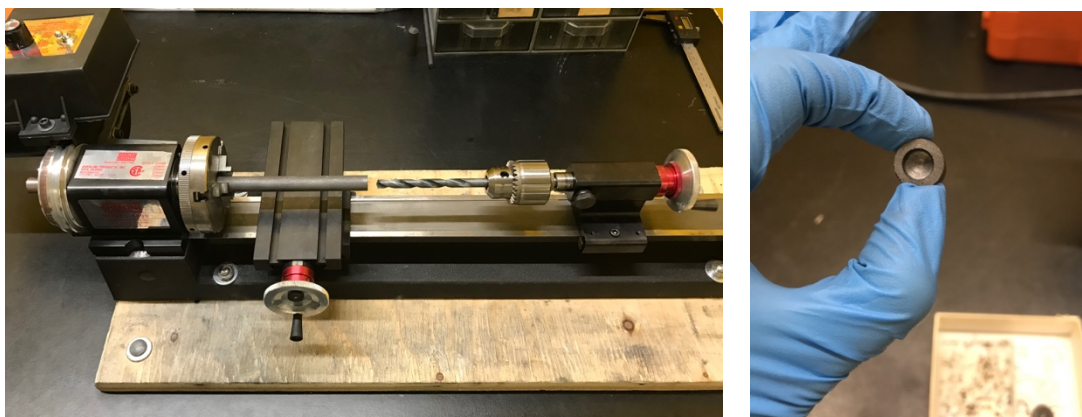
Figure 7 - Photos of graphite capsule production (lathe on the left and the finished capsule on the right)

Figure 8 - Photo of Lindberg-Blue high-temperature furnace

2.2 Thin Section Analysis

Understanding the fluid-bearing phases (micas), from the Sambro Head dyke was a central part of this study. While major and trace element analyses were conducted at the whole rock level, individual crystal examinations were needed to collect geochemical information from the biotite, muscovite, chlorite, and apatite. Three polished thin sections, samples 4-8, 5-4 and 2-2 (Figure 9), all 20 mm by 38 mm were analyzed using petrographic microscopes, EPMA and LA-ICP-MS. Sample 4-8 was selected to be used for data from the mixing zone of the dyke. Samples 5-4 and 2-2 are from two different interior dyke locations, with 2-2 coming from an area that was observed to have a higher concentration of mafic minerals.
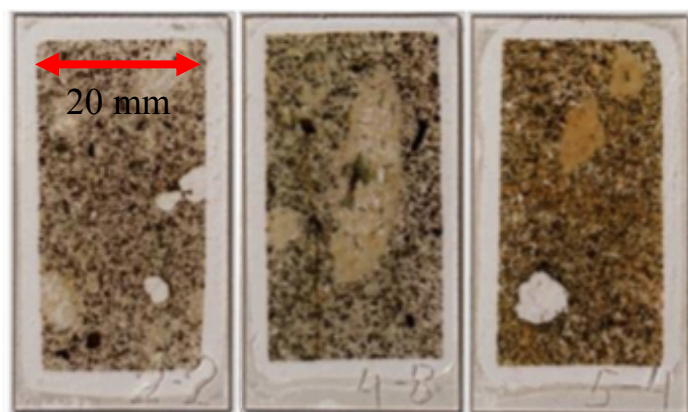
Figure 9 - Scans of thin sections 2-2, 4-8 and 5-4 (left to right)

2.3 Electron Probe Micro-Analyzer (EPMA)

All quantitative major oxide analyses were conducted using the JEOL JXA-8200 Electron Probe Micro-Analyzer 'SuperProbe', in Dalhousie University's Robert M. MacKay Electron Microprobe Laboratory (Figure 10). The EPMA is equipped with five Wavelength Dispersive Spectrometers (WDS) and an Energy Dispersive Spectrometer (EDS) (Weston et al., 1994). The EPMA is capable of measuring most elements from Be to U at high precision (down to trace-element levels of <0.01 wt % for many elements) and can do so simultaneously with five WDS elements and the EDS elements (Weston et al., 1994). The EPMA works by firing a concentrated electron beam at the solid material sample, dispersing X-rays and electrons. Each of

the released X-rays is characteristic of a certain element and is then measured via the WDS and EDS spectrometers. Secondary and back-scattering electrons are also measured to allow detailed surface images and average compositional information to be collected (Reed and Cave, 1995). All measured outputs are referenced against a standardized set of compositions to ensure proper data is being collected. Refer to Table 1 – B1 in Appendix C for all standards used in EPMA analysis. Multiple point analyses were conducted on each sample, both whole rock glasses and thin sections.

Figure 10 - Photo of JEOL EPMA 'SuperProbe' in Dalhousie University's Robert M. MacKay Microprobe Laboratory

The EPMA has micro-scale precision (1 – 5 nm), allowing specific phases to be isolated and analyzed. In situ analysis was performed, allowing any slight variations in chemical composition to be detected within extensively altered crystals. The EPMA is also considered to be a non-destructive method of data collection. This was beneficial when conducting investigations on individual crystals that were later re-analyzed using additional methods (ex. LA-ICP-MS).

2.3.1 Whole Rock and Thin Section Analysis

The whole rock glass samples (pucks 1, 2, and 3), were also analyzed for major oxides and some minor oxides using the EPMA. The specific oxides measured were SiO_2, K_2O, CaO, TiO_2, Al_2O_3, Na_2O, FeO, MgO, MnO, P_2O_5, Cr_2O_3 and BaO. Point analyses using a 10 μm beam size were done in different locations on each glass, with careful attention made to avoid any heterogeneous crystals or elements that might produce discordant data.

Specific biotite and apatite crystals were selected for point analysis, using a 1 μm bean size, in each of the thin sections (4-8, 2-2 and 5-4). Major oxides of interest for these samples were SiO_2, K_2O, CaO, TiO_2, Al_2O_3, Na_2O, FeO, MgO along with MnO, Cr_2O_3, Cl, and F. Multiple intergrown mineral phases were present in the biotite crystals. Extensive chlorite replacement and some muscovite replacement was present, requiring several point analyses from various crystals to ensure the accurate data collection of all three minerals. Apatites within biotite and isolated apatites were selected for point analyses.

2.3.3 X-ray Compositional Mapping

WDS X-ray compositional mapping was conducted on the three thin sections (4-8, 2-2 and 5-4), to illustrate the amount of mineral replacement occurring in the biotites. X-ray compositional mapping is a primary tool for the identification of elemental distribution within a sample. An X-ray map is created through the collection of characteristic X-rays emitted from each element targeted by the electron beam. The WDS measures the released X-rays and rasters the sample under the electron beam to form a compositional mapped image (Friel and Lyman, 2006).

X-ray compositional mapping was used as an additional tool to analyze the extent of chloritization in the biotite crystals from different areas of the dyke. Ti, Mn, F, Cl and Mg were measured from six different biotite crystals. The X-ray maps illustrated which areas of the dyke had the most extensive biotite alteration and gave chemical confirmation that the mixing zone had more chloritization than the interior dyke samples.

Maps of two different biotite crystals were produced for each of the three thin sections. The map resolutions were 250 μm by 250 μm. A beam current of 2.09×10^{-07} Å was used with a 2 μm beam size, and a 100 ms dwell time. This setup allowed for a satisfactory map resolution to be acquired in a reasonable amount of time. Maps for this study were displayed in false colour with a colour scale to represent relative X-ray counts per pixel. Refer to Appendix B for the individual maps.

2.3.4 Backscatter Electron (BSE) Imaging

Several backscatter electron images were taken of the whole rock glasses and thin sections during EPMA analysis. The whole rock glass BSE images were used to determine the number of residual quartz and other heterogeneous areas that remained in the glasses following the fusion process. The primary use of BSE imaging of the polish thin sections was to collect visual data of the number of phases occurring within the biotite crystals. The apatite crystals were also imaged, to investigate growth zoning both within the biotite and in surrounding areas.

BSE imaging is a technique often used to detect multiple chemical phases within a mineral. This is achieved by the sample's interaction with the electron beam, releasing electrons that are then captured by a BSE detector. The BSE images show compositional differences within a sample through the atomic mean number (Reed and Cave, 1993). Brighter elements have a higher atomic mean number, allowing the user to distinguish between minerals and chemical phases.

2.4 Laser Ablation Inductively Coupled Plasma Mass Spectrometry (LA-ICP-MS)

Quantitative trace element data was collected using Laser Ablation Inductively Coupled Plasma Mass Spectrometry (LA-ICP-MS) at Dalhousie University's Health and Environmental Research Centre (HERC) Lab (Figure 11). The HERC Lab houses a Triple Quadropole (TQ) ICP-MS that is attached to a Nd:YAG laser with a 213 nm wavelength. This unit was used to perform all the laser ablation analyses for both the whole rock glasses and thin sections. The LA-ICP-MS operates by focusing a laser onto a substrate and vaporizing (ablating) the surface material. The ablated surface material is carried into the ICP-MS where it is ionized in the plasma torch, before the ions enter the mass spectrometer for measurement.

Thin section biotite analysis was done at 20% energy with a 5 Hz laser repetition rate. A 10 μm spot size, directed in a line scan, was used on various biotite crystals in all three thin sections (4-8, 2-2, and 5-4). Whole rock glasses were run at 50% energy with a 10 Hz laser repetition rate. The glasses were ablated using a 50 -100 μm spot size. Several points were analyzed per glass to ensure homogeneous sampling. All analyses were conducted within a 140 second run time, with 20 seconds allotted for background analysis and flushing of the ablation

cell with helium gas, followed by 60 seconds of laser ablation and 60 seconds of measurement. NIST610 was used as a glass standard for both whole rock glass and thin section analyses. The NIST610 standard was measured twice prior to sample data collection, every 16 samples, and again following sample data collection to record drift. Data reduction was done using IgorPro and integrated Iolite software. Appendix C contains all laser ablation data.
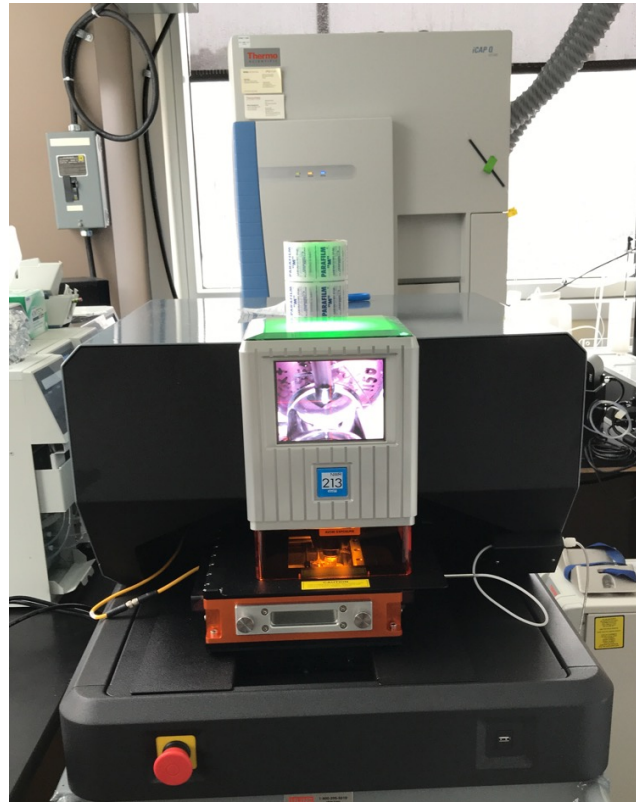
Figure 11- LA-ICP-MS unit (laser located in the front and ICP-MS located at the back)

23

Chapter 3: Whole Rock and Thin Section Results

3.1 Mineralogy and Petrology

Each of the three thin sections (4-8, 2-2, and 5-4), was observed in plain polarized and cross-polarized light using a Nikon ECLIPSE 50iPOL petrographic microscope. General mineralogy across the dyke was found to be plagioclase + quartz + biotite + K-feldspar + apatite + oxides with secondary chlorite ± muscovite. Biotite from each of the sampling locations exhibited chlorite replacement, with more extensive replacement occurring in the mixing zone. BSE imaging was used to identify different phases within and around the biotite. The following BSE images (Figures 12, 13, and 14), illustrate the mineralogy of each dyke sample.
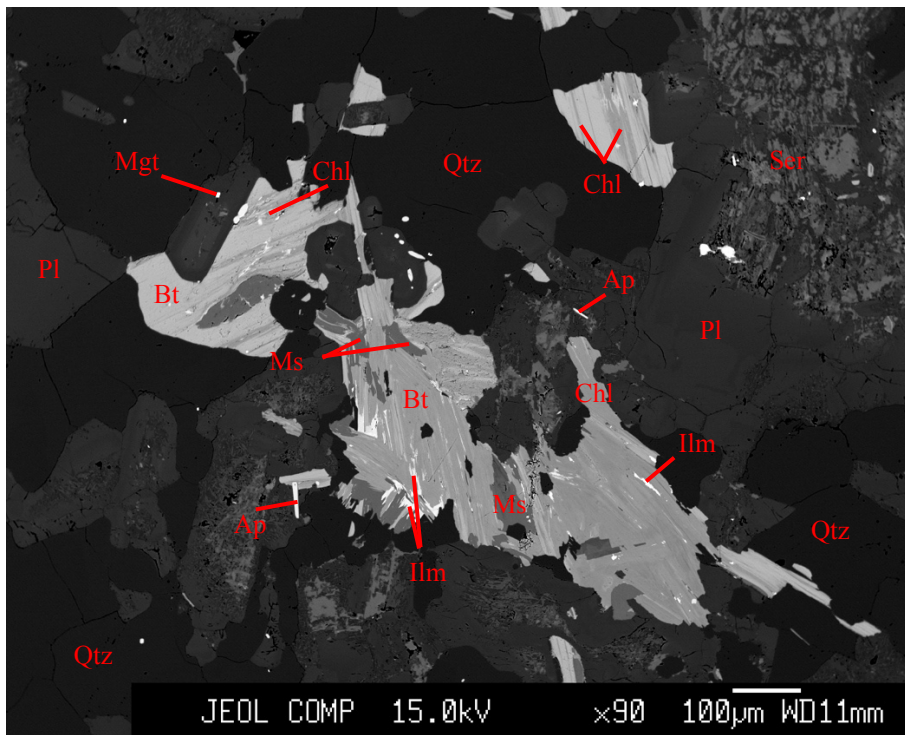
Figure 12 - BSE image of sample 4-8 (mixing zone). Extensive alteration is present with chloritization of the biotite and sericitization of the plagioclase.
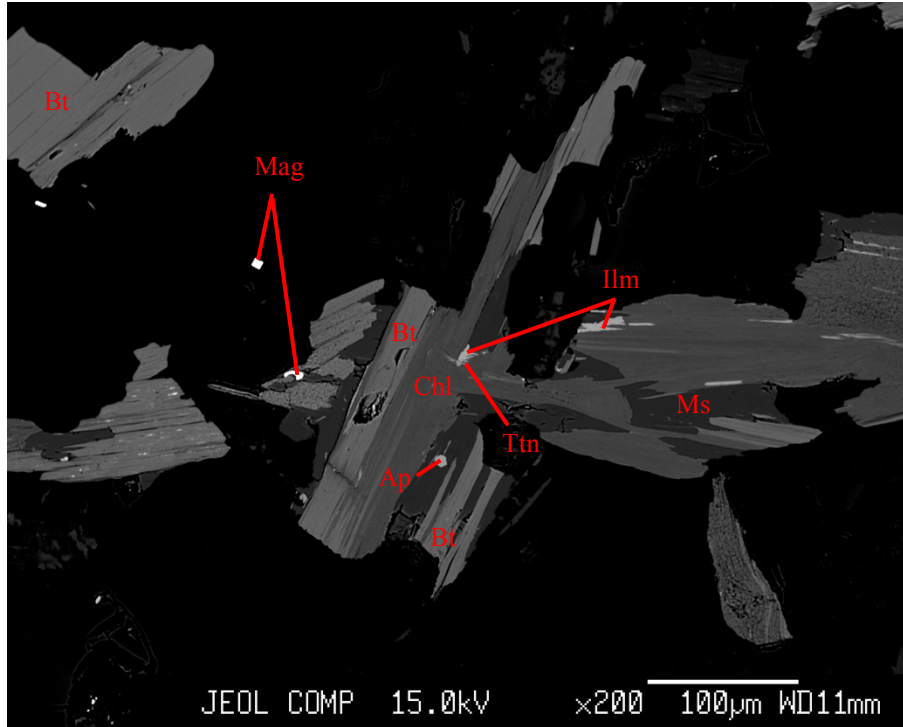
Figure 13 - BSE image of sample 2-2 (central portion of the dyke). This sample displays less mineral alteration, with chloritization of the biotite still present.
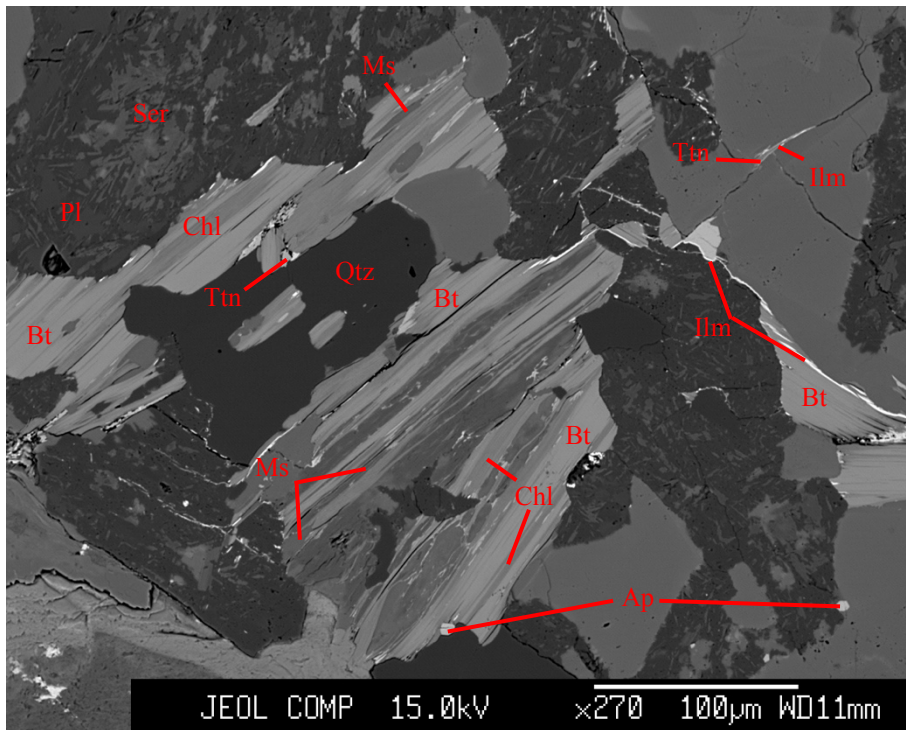
Figure 14 - BSE image of sample 5-4 (central portion of the dyke). Sericitization of the plagioclase and chloritization of the biotite are present. Titanite and ilmenite are found bordering the plagioclase.

Chloritization can be observed consistently throughout the dyke. Chlorite and muscovite replacement occurs along the cleavage planes of the biotite. This indicates that fluid was present in the magma and continued to cause extensive reaction and alteration of biotite long after the dyke had crystallized. Extensive biotite alteration can also be seen in the mixing zone sample 4-8 (Figure 12), where the most fluid reactions appear to have occurred.

Sericite, a fine white mica, is present in the cores of plagioclase crystals throughout the dyke. Sericitization of the plagioclase is another indicator of fluid activity in the magma, which continued at lower temperatures. The sericitization occurring in these dyke samples appears to be mid-to-late stage, causing the plagioclase crystals to appear speckled (Figures 12 and 14). The release of potassium during the chloritization process of the nearby biotite is one possible cause for the late-stage sericitization.

Cordierite, partially altered to pinite, was found in the mixing zone samples 4-8 and 3-3. This is evidence to support the presence of hydrous fluids during the assimilation of the adjacent peraluminous granites with the dyke magma. Erdmann et al. (2009), discovered that in the monzogranite zones of the South Mountain Batholith, where K-feldspar megacrysts are abundant, cordierite is also present. Therefore, the presence of cordierite in the Sambro Head dyke is expected, due to the extent of the magma mixing, and does not require direct contamination from the adjacent metasedimentary rock.

Biotite reaction rims are present along the margins of the K-feldspar megacrysts, indicating disequilibrium with the melt. Titanite and ilmenite are present together in various crystals across the dyke. Figure 14 illustrates the two minerals found interstitially between the biotite and K-feldspar. Magnetite is another mineral present throughout the dyke. It appears frequently in the matrix of the dyke but is also found in plagioclase cores (Figure 12 and 13).

Apatite is a very common mineral found in the dyke. The apatite crystals range in size from 10-100 μm and appear to be primary. Fluorapatites ($Ca_5(PO_4)_3F$) were identified as the primary apatite using EPMA and petrographic observations (notably, c-axis orientations). Figure 15 shows the varieties of apatite crystals found.
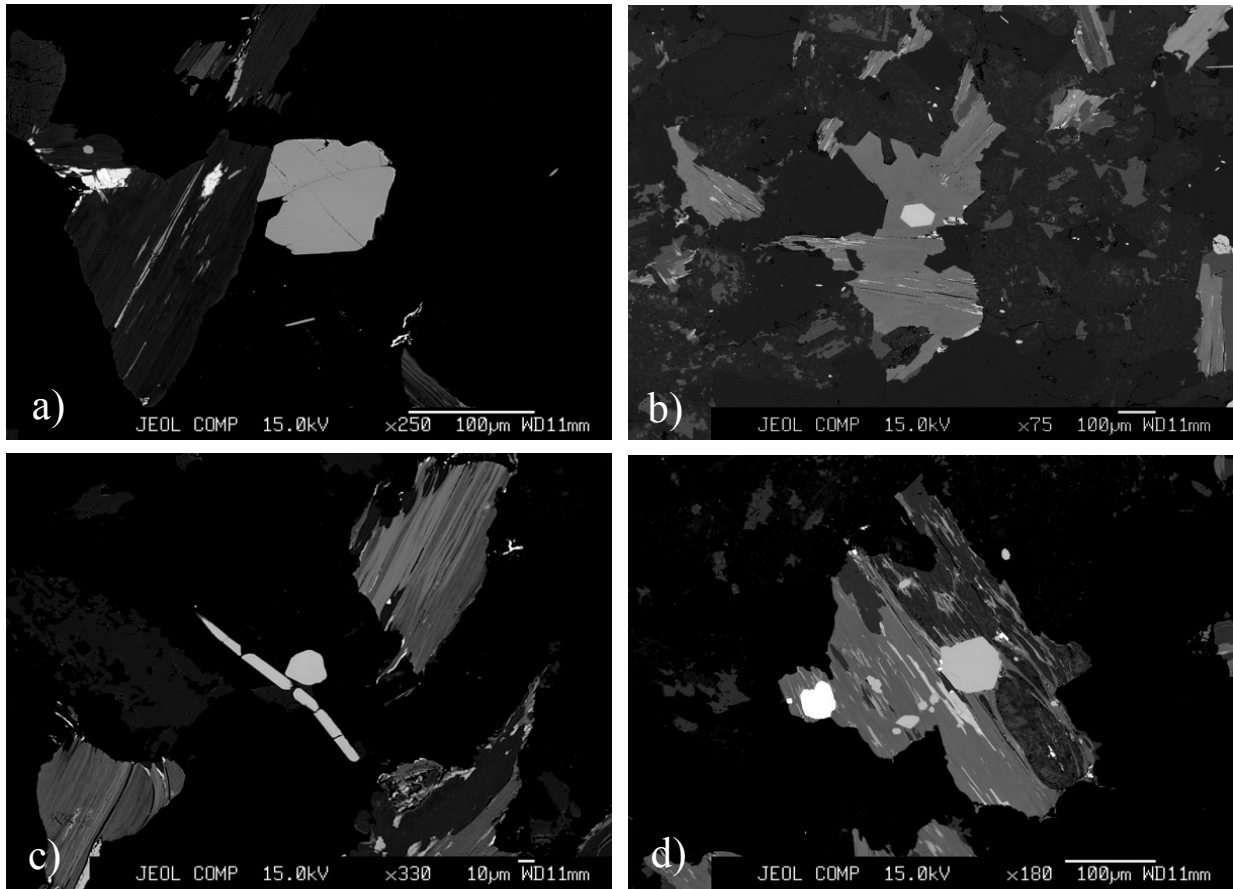
Figure 15 - Apatite crystals from the Sambro Head dyke a), b) and c) are from sample 5-4 (central dyke), and d) is from sample 4-8 (mixing zone)

3.2 Whole Rock Results

3.2.1 Major Elements

Major element analyses were conducted on the whole rock glasses from the Sambro Head dyke and adjacent granites from Peggy's Cove and Prospect, Nova Scotia. Table 1 contains the relationship between the sample names and their sampling location. Table 2 shows the average major element data from each whole rock sample.

Table 1 - Sample names and locations

Sample Name	Sample Location
3DKT2-4-1	Interior Dyke
3DKT7-3-1	Interior Dyke
3DKT1-4-1	Interior Dyke
3DKT2a-036-1	Prospect
2DKT1-036-1	Peggy's Cove
1DKTAll-4-4-1	Mixing Zone
1DKTB-4-3-1	Mixing Zone
1DKTM-4-3-1	Mixing Zone
1DKTT-4-3-2	Mixing Zone
2DKTL-3-2-2	Edge of Mixing Zone

Table 2 - Averaged whole rock major element data

Sample Names	1DKTAl1-4-4-1	1DKTB-4-3-1	1DKTM-4-3-1	1DKTT-4-3-2	2DKTL-3-2-2	3DKT7-3-1	3DKT2-4-1	3DKT1-4-1	3DKT2a-036-1	2DKT1-036-1
Location	Mixing Zone	Mixing Zone	Mixing Zone	Mixing Zone	Edge of Mix. Zone	Central Dyke	Central Dyke	Central Dyke	Prospect	Peggy's Cove
Majors (wt%)										
SiO_2	71.66	72.87	73.32	74.93	72.55	71.59	73.41	72.49	66.24	70.62
TiO_2	0.392	0.433	0.452	0.380	0.293	0.527	0.384	0.458	0.531	0.537
Al_2O_3	15.97	15.66	15.16	14.80	14.71	16.09	14.45	15.79	18.07	16.36
FeO	2.632	2.403	2.875	1.979	2.335	1.926	2.762	2.216	3.143	2.201
MnO	0.131	0.129	0.099	0.094	0.067	0.084	0.071	0.077	0.093	0.095
MgO	1.701	1.821	1.402	1.486	1.311	1.948	1.701	2.189	1.256	1.266
CaO	1.369	1.155	1.290	1.048	0.808	1.569	1.649	1.281	2.391	1.262
Na_2O	2.317	2.165	2.185	2.144	2.715	2.399	2.075	2.275	2.646	2.455
K_2O	2.723	2.321	2.456	2.226	4.538	3.359	2.437	2.668	4.939	4.652
P_2O_5	0.092	0.090	0.117	0.148	0.123	0.124	0.128	0.138	0.139	0.203
Total	98.987	99.05	99.36	99.24	99.45	99.616	99.067	99.582	99.448	99.651
Mg	0.042	0.045	0.035	0.037	0.033	0.048	0.042	0.054	0.031	0.031
Fe	0.037	0.033	0.040	0.028	0.033	0.027	0.038	0.031	0.044	0.031
$Mg= \frac{(100*Mg)}{(Mg + Fe)}$	53.532	57.461	46.501	57.240	50.020	64.323	52.331	63.779	41.600	50.625

The above data shows differences in the major oxide counts across the dyke and between the related granites. Sample 2DKTL-3-2-2, from the outer edge of the Sambro Head dyke (heavily mixed with the adjacent granite), has higher levels of K_2O and lower levels of CaO, MnO, TiO_2 than the rest of the dyke. The mixing zone sample 1DKTB-4-3-1 has the lowest P_2O_5 count of all the whole rock samples. 1DKTB-4-3-1 and 1DKTAll-4-4-1 have the highest counts of MnO. Mg ratios were calculated for all the whole rock sample and reveal clear enrichment of Mg within the dyke. Figure 16 illustrates the variation in MgO concentration. There is a decrease of Al_2O_3 and an increase of SiO_2 in the dyke samples (Figure 17).
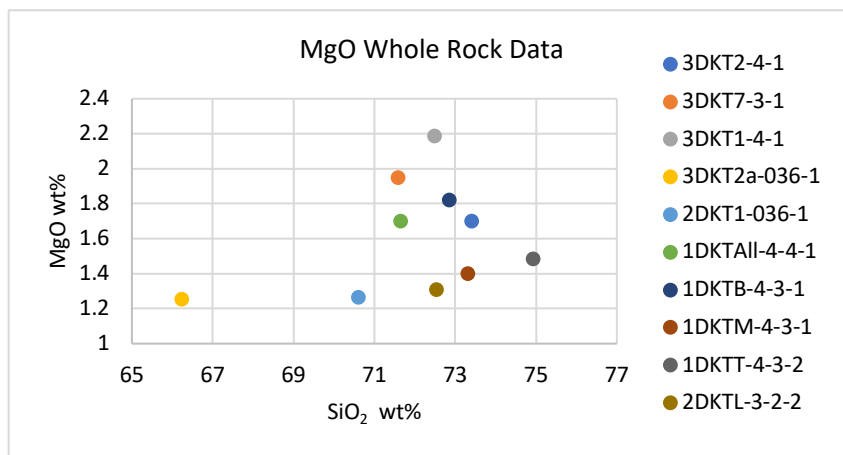
Figure 16 - Whole rock MgO major oxide data
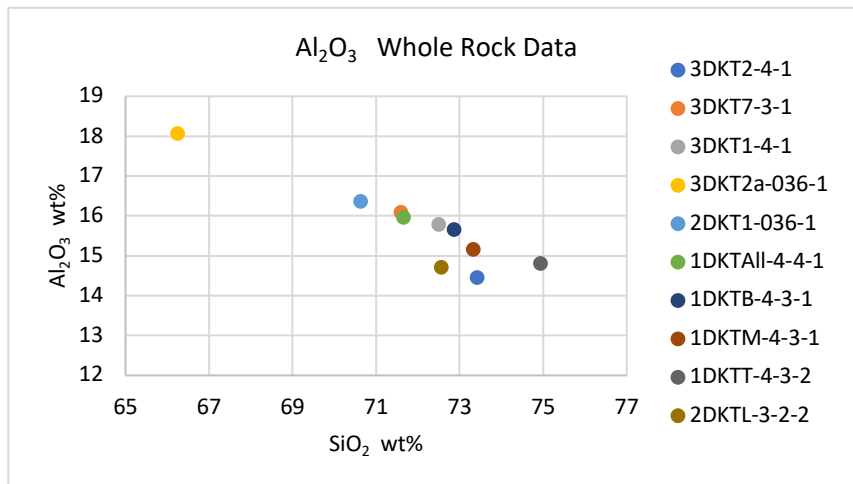
Figure 17 - Whole rock Al₂O₃ major oxide data

3.2.2 Minor and Trace Elements

Eight whole rock samples from the Sambro Head dyke, along with two additional granite whole rock samples from Prospect and Peggy's Cove, Nova Scotia were analyzed for minor and trace elements using LA-ICP-MS. Rare Earth Element (REE) data was measured for all ten samples and normalized to the Boyton (1984) chondrite data set, taken from Rollinson (1993). Figure 18 contains the normalized sample to chondrite REE diagram for all ten samples.

All ten samples have strong negative Eu anomalies and are enriched in Light Rare Earth Elements (LREE). The Eu anomalies were calculated using $(Eu/Eu^*) = Eu_N/\sqrt{[(Sm_N)*(Gd_N)]}$, where X_N is the chondrite normalized element value. The Eu anomalies range from $0.29 - 0.79$ in mixing zone, $0.47 - 0.79$ in the interior dyke and $0.52 - 0.59$ in the granite samples. The Prospect and Peggy's Cove granites are more enriched in REE's than the dyke. Figure 19 includes the mobile and immobile element data, normalized to the Thompson (1982) chondrite values, taken from Rollinson (1993). Generally, the samples are consistent in element concentration however, there are variations between the samples in Ba, Ta and Hf. The increased Ba levels in sample 3DKT2-4-1 can be attributed to the Ba zoned K-feldspar megacrysts, inherited from the adjacent granite, also present in the Prospect and Peggy's Cove granites. The mixing zone samples are enriched in Ta, while the interior dyke and granite samples are depleted. Hf values vary between the granites and the dyke, with the granite being more depleted. The overall enrichment of mobile elements indicates that extensive fluid exchange was occurring following the intrusion of the Sambro Head Dyke. Table 2 – B2 in Appendix C contains all LA-ICP-MS data.
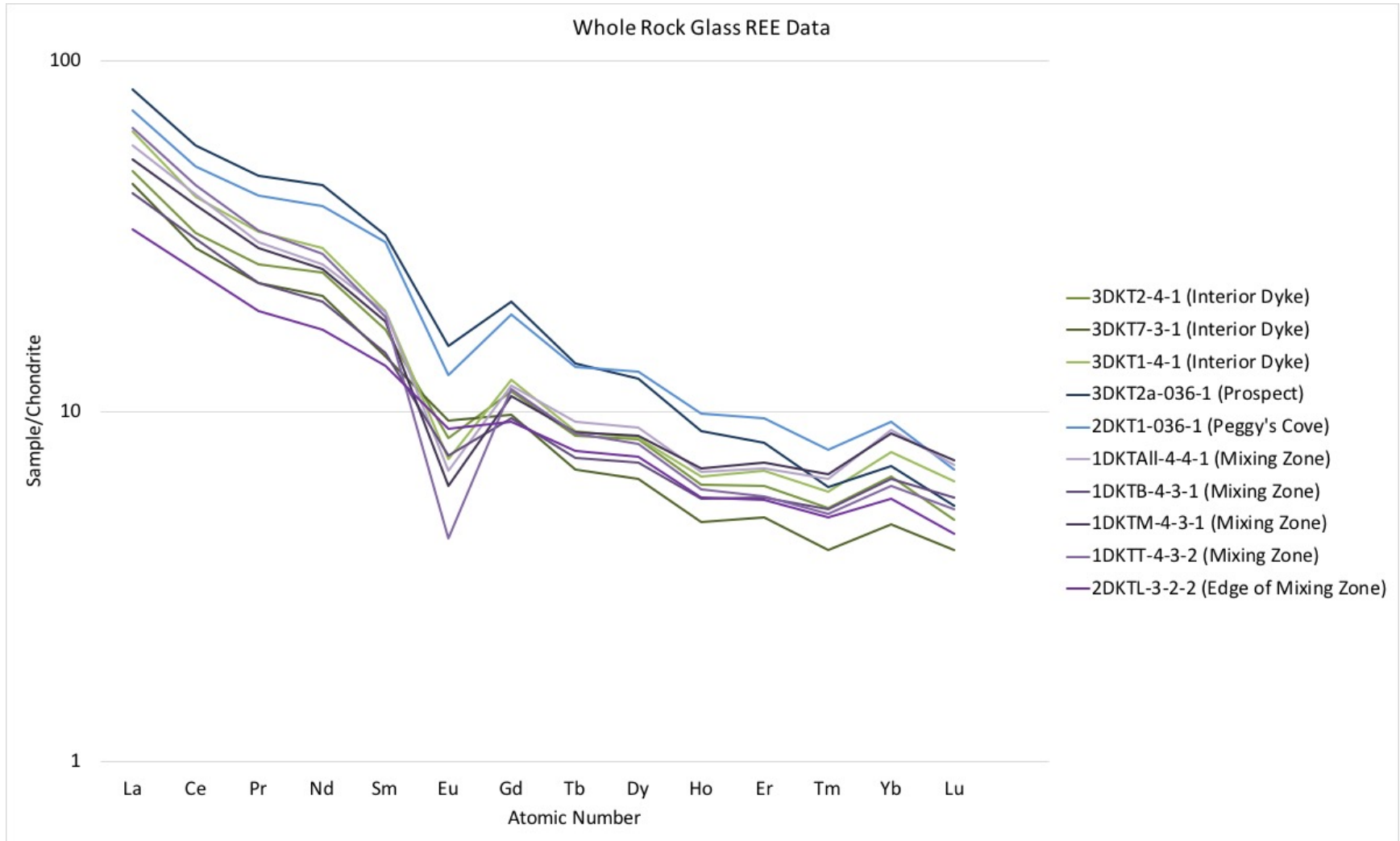
Figure 18 - Whole rock REE plot
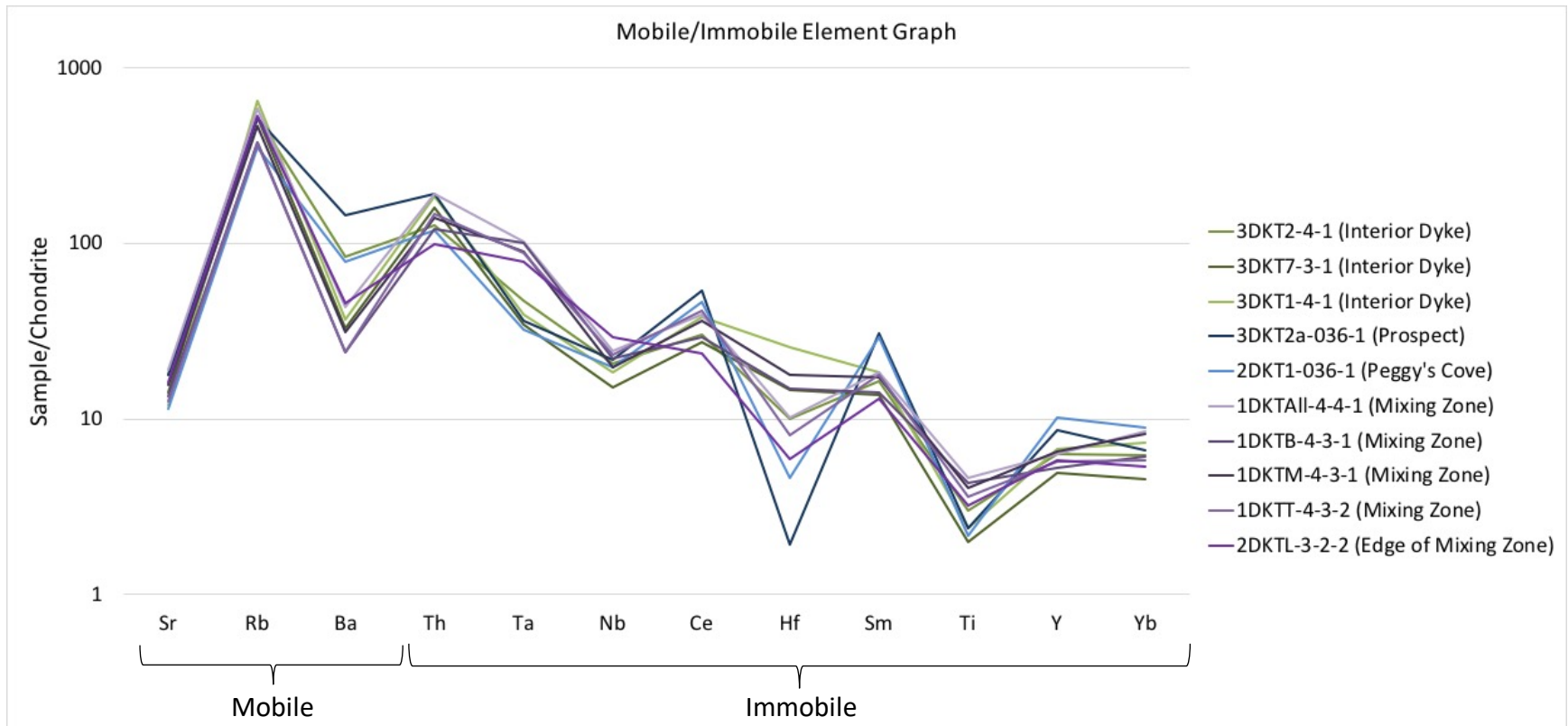
Figure 19 - Mobile/Immobile element graph for whole rock samples

Light Rare Earth Element (LREE) and Heavy Rare Earth Element (HREE) whole rock data are presented in Figures 20 and 21. LREE's from the whole rock dyke samples indicate relative enrichment (Figure 20). The $(La/Sm)_N$ values range from 2.44 – 3.57 with Sm_N ranging from 13.5 – 31.9. Conversely, Figure 21 displays a negative trend of HREE, indicating relative depletion. $(Gd/Yb)_N$ ranges from 1.27 – 2.94 and Yb_N has a range of 4.74 – 9.34. Please refer to Table 1 for the relationship between sample name and sampling location.
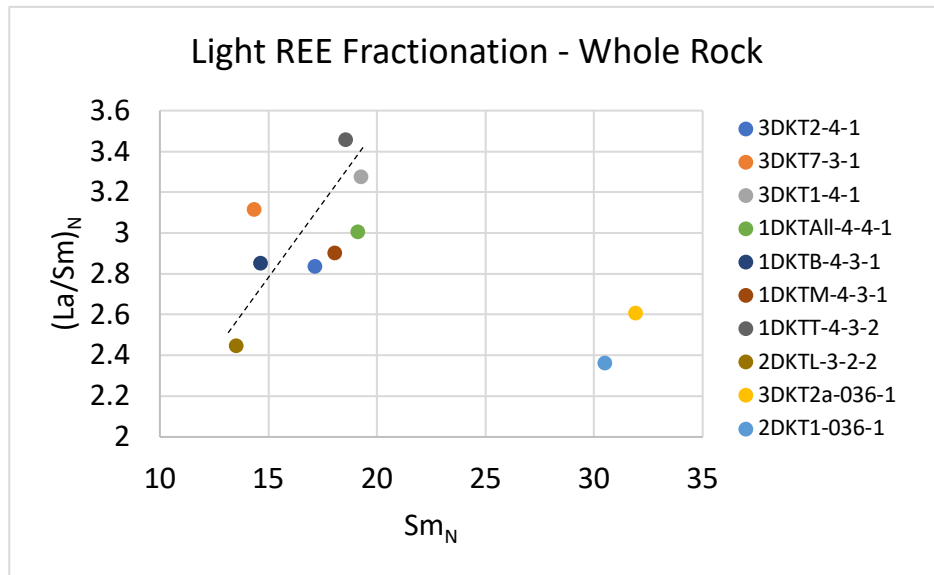
Figure 20 - Whole rock LREE plot showing relative enrichment
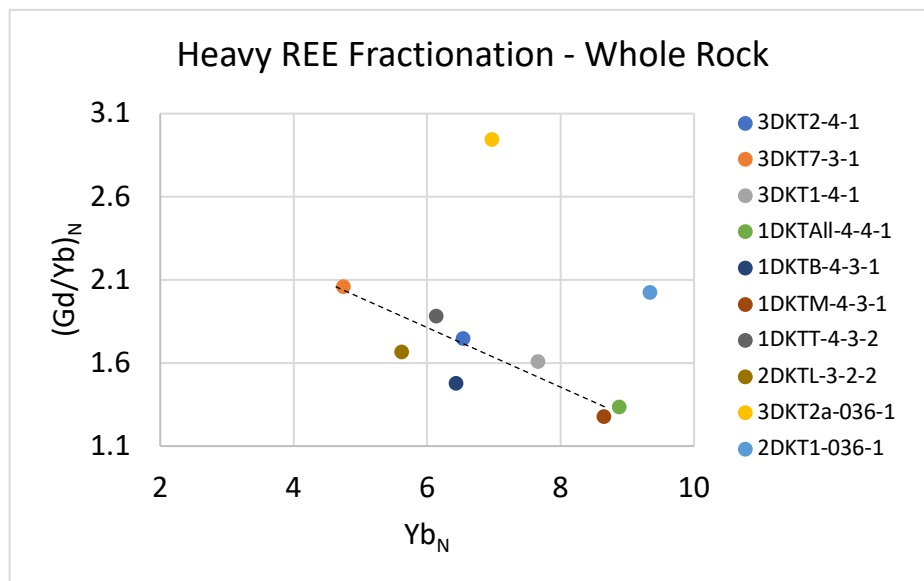
Figure 21 - Whole rock HREE plot showing relative depletion

Figures 22 and 23 indicate enrichment of mobile Large-Ion Lithophile Elements (LILE's) in the dyke. The concentration of Ba in the dyke samples ranges from 163.9 – 989.3 ppm. The Rb concentration ranges from 123.3 – 227.5 ppm and Sr ranges from 99.6 – 211 ppm. The Prospect and Peggy's Cove granite samples are more enriched in both Ba and Sr when compared to samples from the dyke. The relatively consistent variation in Rb, an element enriched in biotite, suggests that the alteration of this mineral was systematic across these rocks.
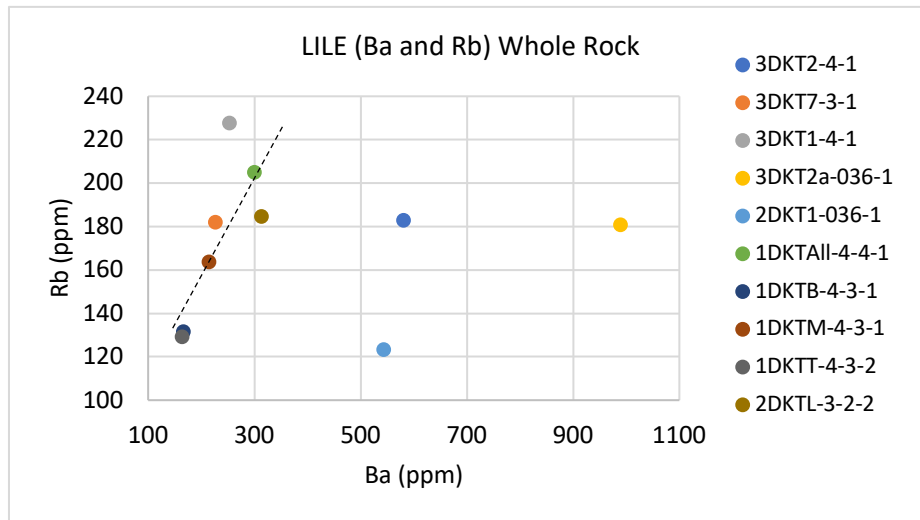
Figure 22 - Ba - Rb whole rock bivariate plot showing the enrichment of LILE's in interior dyke samples
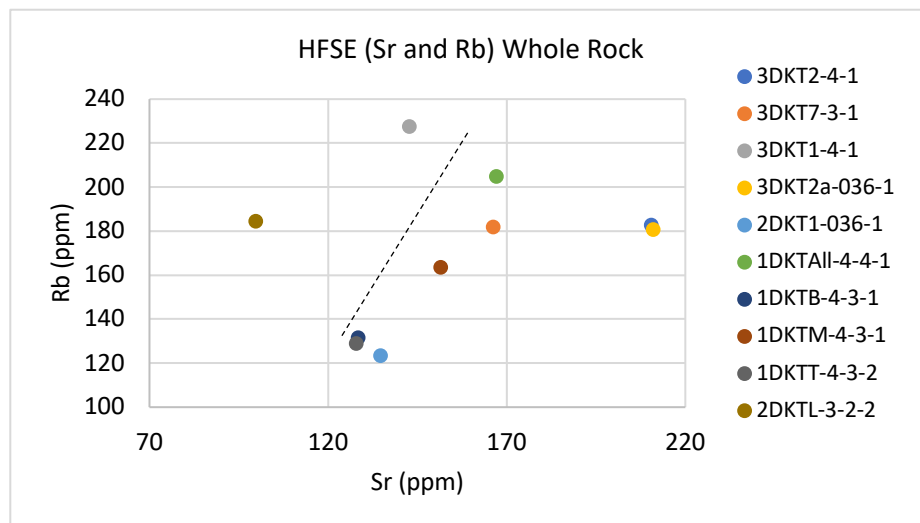
Figure 23 - Sr – Rb whole rock bivariate plot showing the enrichment of LILE's in interior dyke samples

Figure 24 illustrates the distribution of High Field Strength Elements (HFSE's) in dyke samples. Ti ranges from 1851.3 – 2847.5 ppm and Zr ranges from 73.9 – 188.5 ppm. The dyke mixing zone samples show the highest concentrations of HFSE, however, there is considerable variability in both of these elements. As with Rb, Ti is also enriched in biotite, whereas Zr is concentrated by the accessory mineral zircon. The lack of systematic variation in these elements suggests that there may be a process, such as the fluid alteration of biotite, that has resulted in decoupling of Ti and Zr in these rocks.
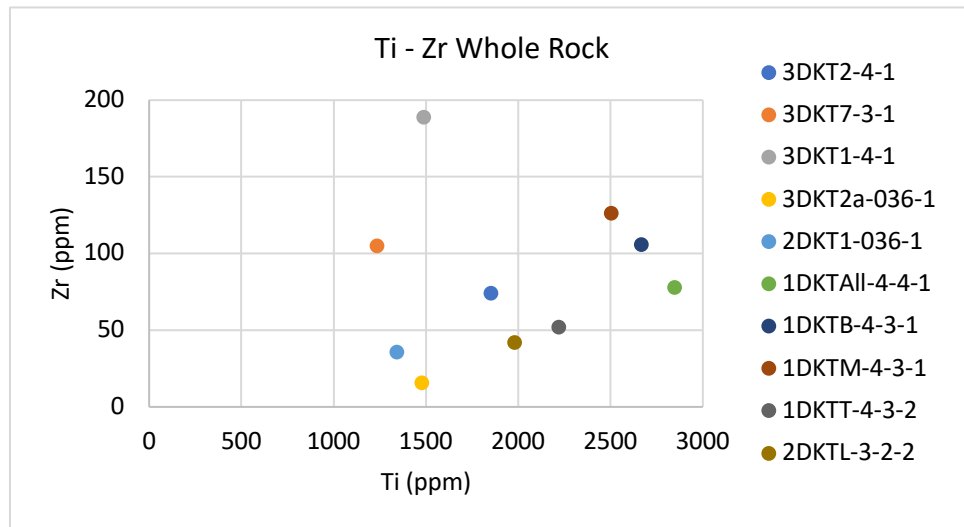
Figure 24 – Zr – Ti bivariate plot showing decoupling of HFSE in the mixing zone samples

3.3 Thin Section Results

3.3.1 Major Element Results

Biotite and apatite crystal were selected and analyzed for major elements from all three thin sections. Thin section major element data was primarily used for geothermometry. Emphasis on the collection of independent biotite, chlorite, muscovite and apatite data was made, as each mineral was needed for separate geothermometry techniques. Chloritization and the extensive replacement of the biotite with additional minerals was taken into account, and the resulting data was carefully separated into mineral specific data (eg. biotite, chlorite and muscovite) for further use. Biotite specific data was collected from the three thin sections, with sample 2-2 (interior

dyke sample) yielding much higher amounts of unaltered biotite. Chlorite was also found in all three samples, with higher quantities found in the mixing zone sample 4-8.

3.3.2 X-ray Compositional Maps of Biotite

Given extensive chloritization present in all of these samples, X-ray compositional mapping was conducted on two biotite crystals from each of the thin sections. The maps were used as a visual tool to assess the extent of biotite alteration across the dyke. Two maps were created for each sample, using biotite crystals located on opposing ends of the thin section. The X-ray compositional maps support observations that have been previously and consistently made in this study: that chloritization is far more extensive in the mixing zone than in the interior dyke. Sample 4-8 (Figure 1 – B1) and sample 5-4 (Figure 3 – B3) from Appendix B, can be used to form a direct comparison. It is clear that far more unaltered biotite is present in sample 5-4. The interstitial replacement of biotite with chlorite is distinct in the map of sample 4-8.

Chapter 4: Geothermometry Procedure and Results

4.1 Purpose of Geothermometry use in this Study

Geothermometry techniques are used to estimate temperatures of formation using fluid-bearing minerals, specifically, biotite, apatite, and chlorite within the Sambro Head dyke. Three geothermometers will be applied to model the local equilibrium and/or disequilibrium of the dyke. A Titanium-in-biotite (TIB) geothermometer will be used to directly assess the effects of varying Ti concentrations on the resulting formation temperatures of biotite. The biotite-apatite geothermometer will apply a different approach, modelling temperatures using the fluorine-hydroxyl exchange between apatite and biotite. A third method, the chlorite geothermometer, will be applied using the Cathelineau (1988) and Jowett (1991) methods, to calculate the formation temperature of chlorite throughout the dyke. The results from these three geothermometry techniques will be evaluated and compared, so as to interpret the conditions and formation temperatures of fluid-bearing minerals within the Sambro Head dyke.

4.2 Ti-in-biotite Geothermometry

A Titanium-in-biotite geothermometer, modelled by Henry et al. (2005), was used to create a temperature profile for this study. TIB geothermometers are known to be a useful tool when interpreting local equilibrium and/or disequilibrium. This geothermometer is recommended for use on peraluminous metapelites that contain graphite, ilmenite, and/or rutile, and have formed under pressures of 3-6 kbar (Henry et al., 2005). The granitic rocks which host the Sambro Head dyke are peraluminous and are estimated to have formed under ~3 kbar of pressure (de Albuquerque, 1977). This geothermometer is therefore being used with the knowledge that there may be slight variations in the data, due to the differences in pressure and in rock composition, versus those for which the thermometer was originally calibrated against.

4.2.1 Procedure for Ti-in-biotite Geothermometry

The TIB geothermometer is achieved using the measured $X_{Mg} = Mg/(Mg + Fe)$ vs. Ti concentration, and solved for temperature (°C) using equation (1) and the surface-fit coefficients (Table 3), determined by Henry et al, 2005.

$$T(°C) = \left(\frac{[\ln(Ti) - a - c(X_{Mg})^3]}{b}\right)^{0.333} \quad (1)$$

Table 3 - Surface-fit coefficients from Henry et al., 2005

Coefficient	Value
A	-2.3594
B	4.6482×10^{-9}
C	-1.7283

For this study, biotite was normalized to a recommended 22 anions, with all iron assumed as Fe^{2+}. This geothermometer has an estimated precision of $\pm 12°C$ at temperatures higher than 700°C and $\pm 25°C$ at temperatures lower than 600°C (Henry et al., 2005). Recommended biotite compositions range from $X_{Mg} = 0.275$-1.0 and concentrations of Ti = 0.04-0.6 apfu (Henry et al., 2005). Temperatures for this study were calculated within the recommended parameters and yielded data between 400°C and 746°C. Table 2 – A2 in Appendix A contains all calculated temperatures with their associated parameters.

4.2.2. Ti-in-biotite Geothermometry Results

Major element analyses were conducted on three thin sections from the Sambro Head dyke using the EPMA. The major oxide data was reduced to individual ions in a biotite formula and temperatures were calculated using equation (1), along with the associated calibration data shown in Table 3. Thin sections taken from more central locations within the dyke (2-2 and 5-4), yielded very similar temperatures. Sample 2-2 had an average temperature of $645 \pm 16°C$ and sample 5-4 had an average temperature of $648 \pm 21°C$. The sample 4-8, taken from the mixing zone of the dyke, yielded an average temperature of $521 \pm 46°C$. The temperature variations and the differences in standard errors between the three samples can be attributed to several factors, all discussed in Henry et al. (2005): (1) Minor to extensive biotite alteration can lead to lower Ti concentrations, this is due to chloritization, (2) Low amounts of graphite present within a sample will generally produce reasonable temperatures and ranges consistent with the TIB parameters but will generate larger standard errors, (3) Normalization procedures can also be to blame for the temperature variations. The 22-oxygen atom approach assumes all iron to be Fe^{2+}. This assumption can cause an overestimation in the total number of cations proportional to those of Fe^{3+} (Henry et al., 2005). Figure 25 illustrates the distribution of all of the temperature data

calculated. Two distinct groups are discernible within the graph, one group of data between 600 - 746°C and the other between 400 - 600°C. These groups represent the different temperatures recorded. Samples 2-2 and 5-4 from the centre of the dyke, yielding very similar, higher temperatures, versus sample 4-8 from the mixing zone of the dyke, which records lower temperatures.
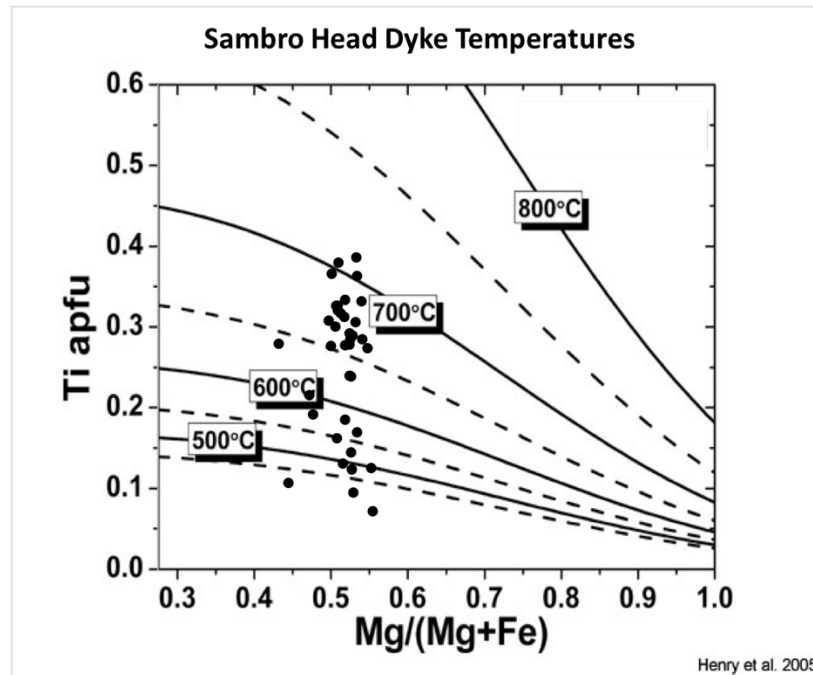
Figure 25 - Graph of all TIB temperature data from the Sambro Head dyke – modified from Henry et al. (2005)

4.3 Biotite-Apatite Geothermometer

The biotite-apatite geothermometer, first modelled by Stormer and Carmichael (1971) and later modified by Ludington (1978), was used in this study to investigate the mineral formation temperatures of biotite and apatite from the Sambro Head dyke. Fluorine and chlorine concentrations within biotite mica are used to estimate the amount of Fl and Cl present in silicate melts (Zhu and Sverjensky, 1992). The biotite-apatite geothermometer is based on the calculation of the partitioning coefficient for the fluorine-hydroxyl exchange between biotite and apatite. This exchange is represented by the following reaction:

$$\tfrac{1}{2}\ KMg_3AlSi_3O_{10}F_2 + Ca_5(PO_4)_3(OH) \quad = \quad \tfrac{1}{2}\ KMg_3AlSi_3O_{10}(OH)_2 + Ca_5(PO_4)_3(F) \quad (2)$$
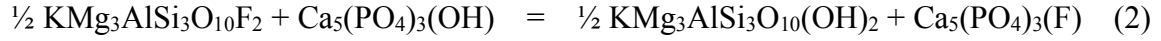
The biotite-apatite geothermometer is known to yield temperatures that are up to ~200°C lower than those produced using alternative geothermometry methods (Yavuz, 1998). This is further explained by Boudreau et al., (1995) and suggests that Ti in biotite could be the cause of the lower temperature yields.

4.3.1 Procedure for Biotite-Apatite Geothermometry

Major oxides from biotite and apatite, collected using the EPMA, were normalized to 22 and 25 anions respectively. The mole fraction, X, was calculated for F and OH in both biotite and apatite, with $X_{Fe} = (Fe + Al^{VI})/ (Fe + Mg + Al^{VI})$ calculated additionally for biotite. The partitioning coefficient, $K_{D,F}$, was calculated using equation (3) from Zhu and Sverjensky (1992):

$$K_{D,F} = \frac{(X_F/X_{OH})^{apatite}}{(X_F/X_{OH})^{biotite}} \quad (3)$$

Temperatures were then calculated using equation (4) from Zhu and Sverjensky (1992):

$$T(°C) = \left(\frac{8852 - 0.024P\ (bars) + 5000X_{Fe}}{1.987 \ln K_{D,F}^{Ap/Bt} + 3.3666} \right) - 273.15 \quad (4)$$

Equation (4) was modelled using linear approximation and has a strict temperature range of 300 – 1100°C, meaning all temperatures that fall above or below these values are inconsistent and should be disregarded (Zhu and Sverjensky, 1992).

4.3.2 Biotite-Apatite Geothermometry Results

The resulting temperatures from the biotite-apatite geothermometer were generally lower than those produced using the Ti-in-biotite geothermometry method. Although the biotite-apatite geothermometer is known to produce temperatures ~200°C lower than those calculated using other methods (Yavuz, 1998), the results are still within a reasonable range for these rocks. The mixing zone (4-8) had a calculated temperature range of 406 – 537°C. The interior dyke (5-4)

had a temperature range of 397 – 547°C, with the other interior dyke sample (2-2) producing a temperature range of 427 – 662°C. Figure 26 is taken from Zhu and Sverjensky (1992), and graphs ln $K_{D,F}$ values against the calculated temperatures in degrees Celsius. This graph is used to show the accepted contours of X_{Fe} and is a visual representation of equation (4).
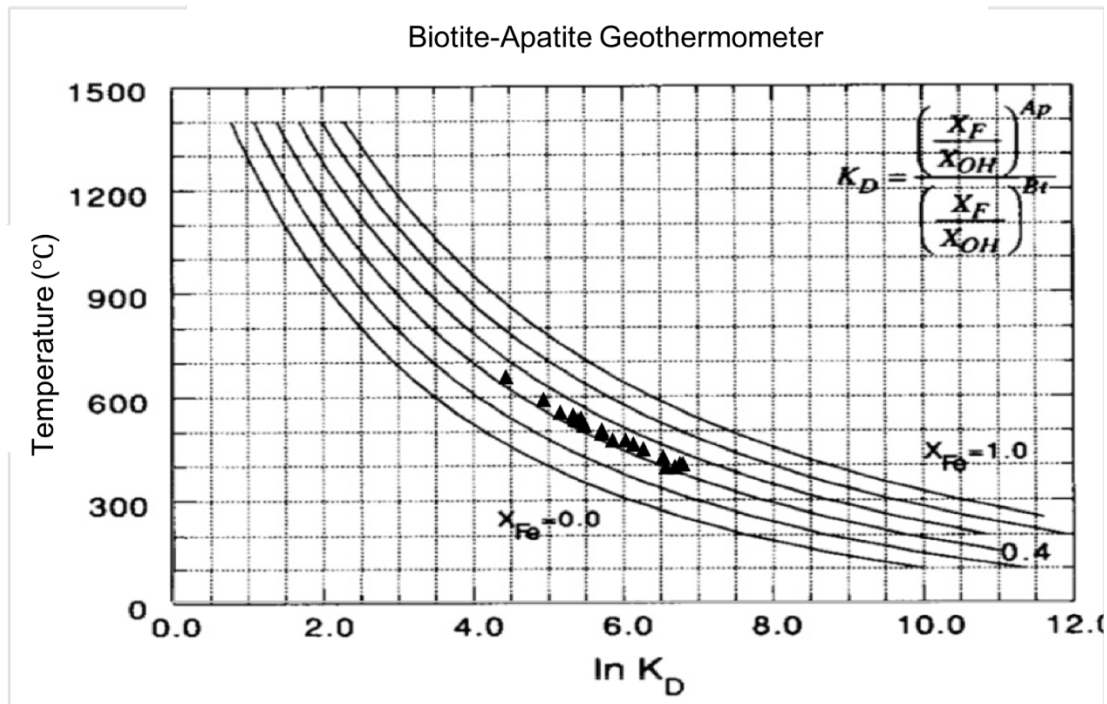
Figure 26 – A modified graph from Zhu & Sverjensky of acceptable X_{Fe} contours for proportional temperature data

All temperature data calculated using the biotite-apatite method lies between the 0.4 - 0.5 X_{Fe} contour, meaning that the temperature data calculated for this study is feasible and meets all the parameters for acceptable temperature yields as recommended by Zhu and Sverjensky (1992). The range of temperatures recorded is lower than for TIB. This suggests volatile exchange between biotite and apatite continued after crystallization. Table 3 – A3 in Appendix A includes all calculations for the biotite-apatite geothermometer.

4.4 Chlorite Geothermometry

Deer at al. (1966), described chlorite as a mineral that can be found in many geologic environments, including sedimentary, low-grade metamorphic, and hydrothermally altered. Two variations of a solid-solution chlorite geothermometer were implemented in this study to determine the temperatures of chlorite in the hydrothermally altered biotite from the Sambro Head dyke. The Cathelineau (1988) and the later improved Jowett (1991) methods, were used to calculate the chlorite formation temperatures. Both of these methods use empirical calibrations established using the positive dependence of Al^{IV} and the variation in Fe/(Fe + Mg). Cathelineau (1988) found a correlation between the Al^{IV} and precipitation temperature and was able to model it using a linear relationship. Chlorite geothermometers are generally thought to be useful between the temperatures of 25 - 350°C, however, they are also prone to inaccuracies as described by de Caritat et al. (1993). Peraluminous bulk rock assemblages have been shown to impact the Fe/(Fe + Mg) field of the geothermometers, yielding overestimated temperatures for both the Cathelineau (1988) and the Jowett (1991) methods, while underestimating temperatures for alternative methods such as those proposed by Kranidiotis & MacLean (1987) in de Caritat et al. (1993). Chlorite geothermometry has therefore been used with caution and in conjunction with the Ti-in-biotite and biotite-apatite geothermometry methods to constrain lower-temperature, fluid reaction temperatures recorded in the Sambro Head dyke.

4.4.1 Procedure for Chlorite Geothermometry

Major oxide data collected from the chlorite was reduced to a half-cell structure, to isolate the tetrahedral atom Al^{IV}. The Cathelineau method models the linear relationship between Al^{IV} and precipitation temperature. The first rendition of the chlorite geothermometer came from Cathelineau and Nieva (1985), see equation (5).

$$T(°C) = 213.3 \, (Al^{IV}) + 17.5 \quad (5)$$

It was later modified by Cathelineau (1988) with a new derivation, see equation (6). The second rendition by Cathelineau (1988) was used in this study as one version of the chlorite geothermometer.

$$T(°C) = -61.92 + 321.98(Al^{IV}) \qquad (6)$$

An additional adaptation was made to the Cathelineau (1988) method by Kranidiotis & MacLean (1987). Their method included the variation of (Fe/(Fe + Mg)) in chlorite and calculated Al^{IV}_C using equation (7) and further calculated the temperature using equation (8).

$$Al^{IV}_C = (Al^{IV}) + 0.7 \, (Fe/(Fe + Mg)) \qquad (7)$$

$$T(°C) = 106 \, (Al^{IV}_C) + 18 \qquad (8)$$

The adapted Cathelineau (1988) equation, by Kranidiotis & MacLean (1987), was further modified by Jowett (1991). Equation (9) is calculated for the tetrahedral Al^{IV}_C and equation (10) applies the Al^{IV}_C parameter, along with the predetermined temperature variables derived by Jowett (1991) to calculate a chlorite formation temperature.

$$Al^{IV}_C = Al^{IV} + 0.1 \, (Fe/(Fe + Mg)) \qquad (9)$$

$$T(°C) = 319 \, (Al^{IV}_C) - 69 \qquad (10)$$

The adaptation by Jowett (1991) was used in this study as the second chlorite geothermometer. The Kranidiotis & MacLean (1987) method was not used in this study as it yields consistently lower temperatures. De Caritat et al. (1993) claim the Jowett (1991) method is best applied to chlorites with (Fe/(Fe + Mg)) values < 0.6. Since the chlorite from the Sambro Head dyke has an (Fe/(Fe + Mg)) of 0.5 on average (from preliminary calculations), the Jowett method was used in this study.

4.4.2 Chlorite Geothermometry Results

Temperatures calculated using the Cathelineau (1988) and Jowett (1991) methods produced chlorite temperature ranges congruent with low-temperature formation conditions. Table 4 – A4 and Table 5 – A5 in Appendix A, have the complete set of temperatures calculated using both methods for all three dyke samples. Chlorite found in the mixing zone from sample 4-8, produced a temperature range of 242 – 368°C with an average temperature of 325°C using the

Cathelineau (1988) method, and a range of 245 – 373°C with an average temperature of 330°C using the Jowett (1991) method. Interior dyke samples, 5-4 and 2-2, yielded lower temperatures than in the mixing zone. The temperature range of sample 5-4 was 224 – 386°C with an average temperature of 293°C using the Cathelineau (1988) method, and 228 – 386°C with an average temperature of 297°C using the Jowett (1991) method. The calculated temperature range for sample 2-2 was 286 – 333°C with an average temperature of 314°C using the Cathelineau (1988) method and 290 – 336°C with an average temperature of 319°C using the Jowett (1991) method.

The minor variations in temperatures recorded can be attributed to the amount of chloritization occurring across the dyke, rather than any major differences in fluid temperatures. The mixing zone has higher chlorite content than the interior dyke samples as it was subjected to more hydrothermal alteration. The amount of chlorite analyzed using EPMA also varies across the three samples. Due to the extensive chloritization in the mixing zone, far more chlorite data was collected from sample 4-8. Smaller numbers of chlorite were analyzed in samples 5-4 and 2-2. On average, the Jowett (1991) method yielded temperatures that were only slightly higher than the Cathelineau (1988) method. This slight temperature difference indicates that there is not a significant variation in Fe and Mg content in the chlorite. Furthermore, all of the rocks have clearly continued to undergo fluid exchange at temperatures of ~300°C. This may account for the unusual final composition of the dyke samples.

Chapter 5: Discussion

5.1 Comparison of Geothermometers

Three different geothermometers were used to model the formation temperatures of the Sambro Head dyke: Ti-in-biotite, biotite-apatite and chlorite geothermometry. The TIB geothermometer was used to calculate the formation temperature of biotite while the biotite-apatite geothermometer most likely represents fluid exchange recorded by biotite and apatite partitioning of F, Cl and OH. The chlorite formation temperature was calculated using chlorite geothermometry and represents the latest stage of high-temperature fluid activity.

Temperature results from the TIB and biotite-apatite geothermometers are comparable, however, two factors must be considered: the temperature deficit for the biotite-apatite method and the limited collection of apatite and biotite from sample 4-8. The biotite-apatite geothermometer is known to yield temperatures ~200°C lower than other biotite geothermometry methods (Yavuz, 1998). Apatite EPMA data for sample 4-8 from the mixing zone was limited. The extensive chloritization in this sample further affected the precision of the biotite-apatite method, as biotite was sparse and minimal EPMA data was collected. Due to these factors only two biotite-apatite calculations were completed for the sample 4-8, limiting the amount of temperature data for this region of the dyke. It is likely that the average temperature from these two calculations is therefore too high. When comparing the data from the other locations of the dyke, both of which contained significant numbers of apatite and biotite for EPMA collection, their temperature trends were congruent with those produced using the TIB geothermometer. Table 4 contains the average temperature data from the three sampling locations for both methods.

Table 4 - Average Ti-in-Biotite and Biotite-Apatite Geothermometer Data

Sample	Average Ti-in-Biotite Temperature (°C)	Average Biotite-Apatite Temperature (°C)
4-8 (Mixing Zone)	520.75	471.92
5-4 (Interior Dyke)	648.33	467.46
2-2 (Interior Dyke)	644.52	524.46

Given the considerations for sample 4-8, this study interprets that the lower biotite formation temperatures were calculated in the mixing zone (sample 4-8), between the dyke and adjacent granite. Higher and more consistent formation temperatures were calculated from the central dyke samples (5-4 and 2-2). The temperature variations within the dyke, using the TIB and biotite-apatite methods, can be attributed to mineralogical and compositional differences. The dyke is heterogeneous and includes areas of varying mineral concentration and mineral alteration.

Chlorite formation temperatures calculated using the Cathelineau (1988) and Jowett (1991) methods yielded higher temperatures in the mixing zone of the dyke. The interior dyke samples (5-4 and 2-2) produced analogous temperatures, lower than those of the mixing zone. The concentration of chlorite varies significantly between the mixing zone and the interior dyke. Hydrothermal fluids were present in higher concentrations along the margins of the dyke and contributed to the extensive chloritization of biotite and the alteration of other minerals, such as the sericitization of plagioclase. Figure 27 illustrates the average temperatures yielded from the three geothermometry techniques as well as their associated standard errors.
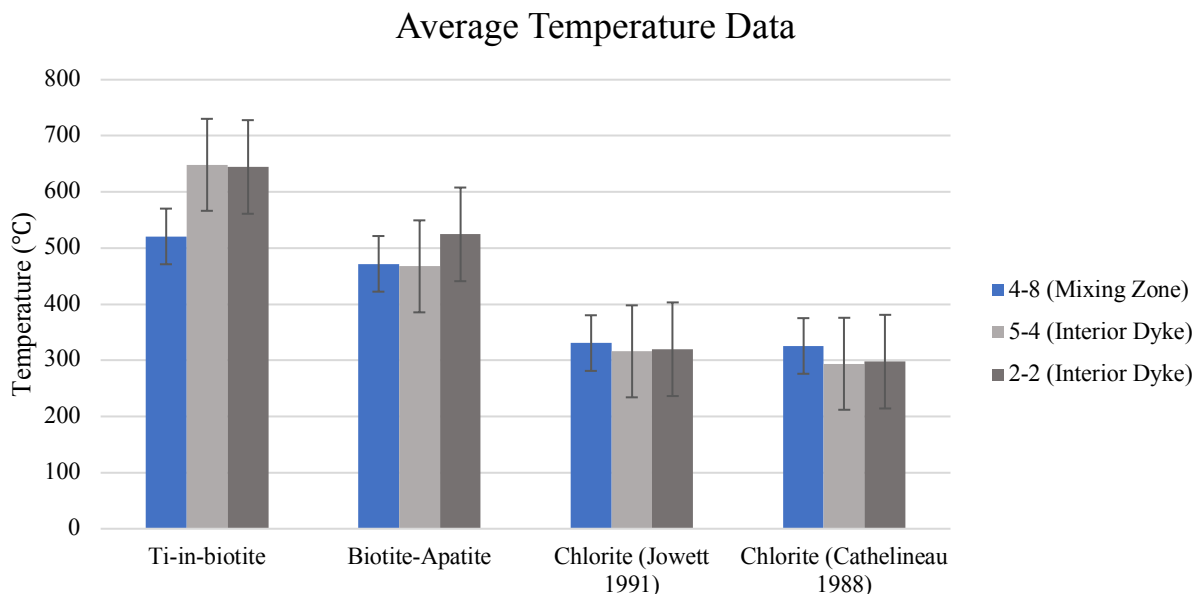
Figure 27 - Average temperature data from all three geothermometry techniques with their associated standard errors

5.2 Petrochemical Modelling

The mineralogy of the Sambro Head dyke consists of plagioclase + quartz + biotite + K-feldspar + apatite + oxides with secondary chlorite ± muscovite. The dyke can be classified as a tonalite, the result of a mafic source that chemically mixed with the South Mountain Batholith biotite-monzogranite. LREE geochemical data supports the hypothesis that the mafic source was likely mantle magma. Based on the results from this study, the Sambro Head dyke is believed to have originated from mantle magma that intruded and mixed with the granite in the Sambro Head region. The evidence for magma mixing is clear, both texturally and chemically and is primarily represented by the inherited, Ba zoned, K-feldspar megacrysts and the enrichment of REE's in the dyke. Other mineralogical indicators such as biotite reaction rims and the presence of cordierite, alerted to pinite, also support magma mixing. The enrichment of LILE's suggests significant fluid exchange occurred in the dyke. The distribution of the HFSE's indicates magma mixing but with considerable decoupling of Zr and Ti.

Temperatures calculated using geothermometry suggest three distinct formation temperatures. The TIB geothermometry results indicate that the peak formation temperature of biotite was ~ 648 °C, suggesting biotite formed at medium to low temperatures conditions during the mixing of the hotter mafic magma with the granitic host. Biotite-apatite results suggest that apatite formation occurred at similar temperatures, with a slightly lower peak formation temperature of ~ 524°C. Temperature calculations from the chlorite geothermometry confirm that chlorite formed during a secondary, low-temperature fluid reaction phase. The chlorite had a peak formation temperature of ~ 325°C. Additional alteration minerals such as sericite are also likely to have formed during this secondary fluid reaction phase.

Chapter 6: Conclusion

6.1 Concluding Statement

This study investigated the fluid exchange reactions between the host granitic rock and the Sambro Head dyke. Extensive geochemical analyses have suggested that the dyke originated from mafic mantle magma and mixed with the biotite-monzogranite of Bald Rock in Sambro Head, Nova Scotia. Large scale mixing/mingling of the mafic intrusion with the host granite is likely to have created related enclaves in the Sambro Head region. Based on the textural and geochemical evidence, it can be concluded that the Sambro Head dyke was the result of hybridization, the mixing of a mafic magma with the granitic host. A brief crystallization history was determined using geochemical and geothermometry results from biotite, apatite and chlorite. The mineral assemblage of this dyke was formed at relatively low-temperatures and altered later by a secondary fluid reaction phase.

6.2 Recommendations for Future Work

Recommendations for future work stemming from this study include:

(1) Further trace-element analysis of the biotite crystals from the different areas of the dyke (specifically looking at Rb, Sr, Pb, Ni, Zr).
(2) The collection of samples from the enclaves surrounding the Sambro Head dyke (progressing away from the dyke), and other related localities to conduct chemical analyses.
(3) Drill core sampling of the Sambro Head dyke, to retrieve fresh, unweathered samples and to gain more insight into the extent of the intrusion.

References

Boudreau, A. E., Love, C., Prendergast, M. D. (1995) Halogen geochemistry of the Great Dyke, Zimbabwe. Contributions to Mineralogy and Petrology. (122): 289-300.

Cathelineau, M. (1988). Cation site occupancy in chlorites and illites as a function of temperature. The Mineralogical Society: Clay Minerals. (23): 471-485.

Cox, R. A., Dempster, T. J., Bell, B. R., and Rogers, G. (1996). Crystallization of the Shap Granite: evidence from zoned K-feldspar megacrysts. Journal of the Geological Society,153 (4): 625-635. doi:10.1144/gsjgs.153.4.0625

de Albuquerque, C. A. R. (1977). Geochemistry of the tonalitic and granitic rocks of the Nova Scotia southern plutons. Geochimica et Cosmochimica Acta (41): 1-13.

de Caritat, P., Hutcheon, I., Walshe, J. L. (1993). Chlorite geothermometry: a review. Clays and Clay Minerals. (41): 219-239.

Erdmann, S., Jamieson, R. A., MacDonald, M. A. (2009). Evaluating the origin of garnet, cordierite and biotite in granitic rocks: a case study from the South Mountain Batholith, Nova Scotia. Journal of Petrology (50): 1477-1503. doi:10.1093/petrology/egp038

Friel, J. J., Lyman, C. E. (2006). X-ray Mapping in Electron-Beam Instruments. Microscopy and Microanalysis: Microscopy Society of America. (12): 2-25. doi:10.1017/S1431927606060211

Henry, D. J., Guidotti, C. V., Thomson, J. A. (2005). The Ti-saturation surface for low-to-medium pressure metapelitic biotites: Implications for geothermometry and Ti-substitution mechanisms. American Mineralogist. (90): 316-328.

Horne, R. J., Macdonald, M. A., Corey, M. C., & Ham, L. J. (1992). Structure and emplacement of the South Mountain Batholith, southwestern Nova Scotia. Atlantic Geology, 28 (1): 29-50. doi:10.4138/1849

Jowett, E. C. (1991). Fitting iron and magnesium into the hydrothermal chlorite geothermometer. GAC/MAC/SEG Joint Annual Meeting, Toronto, 27-29 May, Program with Abstracts 16, A62.

Kranidiotis, P., and MacLean, W.H. (1987). Systematics of Chlorite Alteration at the Phelps Dodge Massive Sulfide Deposit, Matagami, Quebec. Economic Geology (82): 1898-1911. Doi: 0361-0128/87/747/1

Kretz, R. (1983). Symbols for rock-forming minerals. American Mineralogist. (68): 277-279.

Ludington, S. (1978). The biotite-apatite geothermometer revisited. American Mineralogist. (63): 551-553.

MacDonald, M.A. and Clarke, D.B. (2017). Occurrence, origin, and significance of melagranites in the South Mountain Batholith, Nova Scotia. Canadian Journal of Earth Sciences. (54): 693-713. dx.doi.org/10.1139/cjes-2016-0106

Reed, S. and J. B., Cave, M. R. (1995). Microprobe Techniques in the Earth Sciences: Electron Microprobe Analysis. The Mineralogical Society Series, Vol (6): 49-90.

Rollinson, H. (1993). Using geochemical data: evaluation, presentation, interpretation. Routledge: Taylor and Francis Group, New York, NY, USA.

Stashin, S. (2017). Investigating possible hybridization of the Peggy's Cove granite section of the Halifax Pluton, South Mountain Batholith, Nova Scotia. Dalhousie University, Halifax, Nova Scotia

Stormer, J. C., Carmichael, I. S. E. (1971). Fluorine-hydroxyl exchange in apatite and biotite: a potential igneous geothermometer. Contributions to Mineralogy and Petrology. (31): 121-131.

Westerman, D. S., Dini, A., Innocenti, F., Rocchi, S. (2004). When and where did the hybridization occur? The case of the Monte Capanne Pluton, Italy. Atlantic Geology, 39 (2): 147-162.

Weston, P. E., Konnert, J. A., Wolpert, P. J. (1994). JEOL 8900 SuperProbe User's Manual. U.S Department of the Interior U.S Geologic Survey. Open File Report: 94-404.

White, C. E., Barr, S. M. 2012. Meguma Terrane Revisited; Stratigraphy, Metamorphism, Paleontology and Provenance. Journal of the Geological Association of Canada, 39(1).

Wongus, D. (2013). Variations in barium concentrations in K-feldspar zoning, Peggys Cove and Prospect, Nova Scotia (Unpublished BSc Honours thesis). Dalhousie University, Halifax, Nova Scotia.

Yavuz, F. (1998). Short note: BIOAPAG-PC: Program for an apatite and biotite geothermometer. Computers & Geosciences (24): 885-891.

Zhu, C., and Sverjensky, D. A. (1992). F-Cl-OH partitioning between biotite and apatite. Geochimica et Cosmochimica Acta. (56): 3435-3467.

Appendix A – Geothermometry Data

Sample Name	Temperature (°C)	Ti (apfu)	Mg/(Mg+Fe)
Table 2 – A2			
4-8	583	0.192	0.496
4-8	605	0.216	0.491
4-8	404	0.108	0.465
4-8	491	0.124	0.545
5-4	708	0.381	0.528
5-4	534	0.145	0.544
5-4	690	0.334	0.536
5-4	682	0.318	0.530
5-4	504	0.132	0.533
5-4	685	0.327	0.527
5-4	701	0.367	0.519
5-4	674	0.309	0.515
5-4	682	0.321	0.527
5-4	680	0.313	0.535
5-4	685	0.327	0.524
5-4	555	0.163	0.525
2-2	746	0.479	0.560
2-2	668	0.286	0.543
2-2	639	0.241	0.541
2-2	657	0.278	0.518
2-2	664	0.279	0.542
2-2	672	0.302	0.524
2-2	400	0.096	0.546
2-2	706	0.364	0.551
2-2	671	0.290	0.545
2-2	694	0.332	0.557
2-2	588	0.186	0.536
2-2	667	0.275	0.564
2-2	671	0.293	0.541
2-2	714	0.386	0.550
2-2	681	0.307	0.549
2-2	507	0.126	0.569
2-2	645	0.280	0.452
2-2	661	0.278	0.536
2-2	638	0.239	0.544
2-2	575	0.171	0.551
2-2	671	0.286	0.558

Sample	Temperature (°C)	$X_F^{Apatite}$	$X_{OH}^{Apatite}$	$X_F^{Biotite}$	$X_{OH}^{Biotite}$	$X_{Fe}^{Biotite}$	P (bars)	$K_{D,F}$
4-8	537.76	0.893	0.107	0.037	0.963	0.527	3000	218.99
4-8	406.08	0.948	0.052	0.019	0.981	0.547	3000	931.30
5-4	465.44	0.939	0.061	0.031	0.969	0.552	3000	478.23
5-4	399.15	0.883	0.117	0.010	0.990	0.463	3000	743.34
5-4	408.08	0.974	0.026	0.041	0.959	0.541	3000	889.00
5-4	506.15	0.937	0.063	0.045	0.955	0.548	3000	312.32
5-4	397.62	0.941	0.059	0.019	0.981	0.490	3000	837.28
5-4	547.75	0.893	0.107	0.038	0.962	0.544	3000	211.99
5-4	476.53	0.934	0.066	0.032	0.968	0.555	3000	429.28
5-4	538.95	0.889	0.111	0.033	0.967	0.557	3000	238.15
2-2	477.39	0.929	0.071	0.035	0.965	0.508	3000	364.04
2-2	662.53	0.782	0.218	0.040	0.960	0.535	3000	87.04
2-2	558.33	0.856	0.144	0.032	0.968	0.519	3000	179.56
2-2	518.84	0.892	0.108	0.032	0.968	0.511	3000	247.09
2-2	523.79	0.884	0.116	0.030	0.970	0.524	3000	245.69
2-2	427.74	0.958	0.042	0.031	0.969	0.543	3000	706.03
2-2	596.00	0.832	0.168	0.034	0.966	0.543	3000	142.85
2-2	448.74	0.958	0.042	0.040	0.960	0.536	3000	542.04
2-2	535.28	0.921	0.079	0.049	0.951	0.534	3000	228.97
2-2	495.94	0.901	0.099	0.028	0.972	0.518	3000	312.44

Table 3 – A3

Table 4 – A4		
Sample	T (°C)-Cathelineau (1988)	T (°C)-Jowett (1991)
4-8	302.16	306.82
4-8	286.19	289.64
4-8	342.73	348.09
4-8	349.74	354.78
4-8	344.82	349.97
4-8	346.68	351.97
4-8	308.38	313.78
4-8	324.94	330.54
4-8	348.52	353.70
4-8	328.51	334.12
4-8	324.31	329.69
4-8	340.12	345.45
4-8	351.16	357.06
4-8	342.11	348.53
4-8	351.99	358.32
4-8	289.52	295.62
4-8	368.83	373.02
4-8	288.45	293.75
4-8	242.10	245.40
4-8	292.87	298.39
4-8	277.11	281.14
4-8	352.17	357.47
4-8	347.84	353.30
4-8	349.66	353.04
4-8	358.22	363.67
4-8	307.26	312.74
Average T (°C) =	325.63	330.77
SE=	6.15	6.21

Table 5 – A5		
Sample	T (°C)-Cathelineau (1988)	T (°C)-Jowett (1991)
5-4	235.62	239.90
5-4	269.05	272.61
5-4	295.32	299.30
5-4	320.84	325.31
5-4	305.97	310.11
5-4	322.78	327.75
5-4	283.38	287.67
5-4	283.90	287.98
5-4	251.13	254.50
5-4	224.99	228.45
5-4	386.29	386.75
5-4	341.47	345.58
5-4	299.80	304.04
Average T (°C) =	293.89	297.69
SE=	12.23	12.12
2-2	286.48	290.03
2-2	333.10	336.98
2-2	317.45	321.73
2-2	327.14	330.47
Average T (°C) =	316.04	319.81
SE=	10.37	10.40

Appendix B – X-ray Compositional Maps

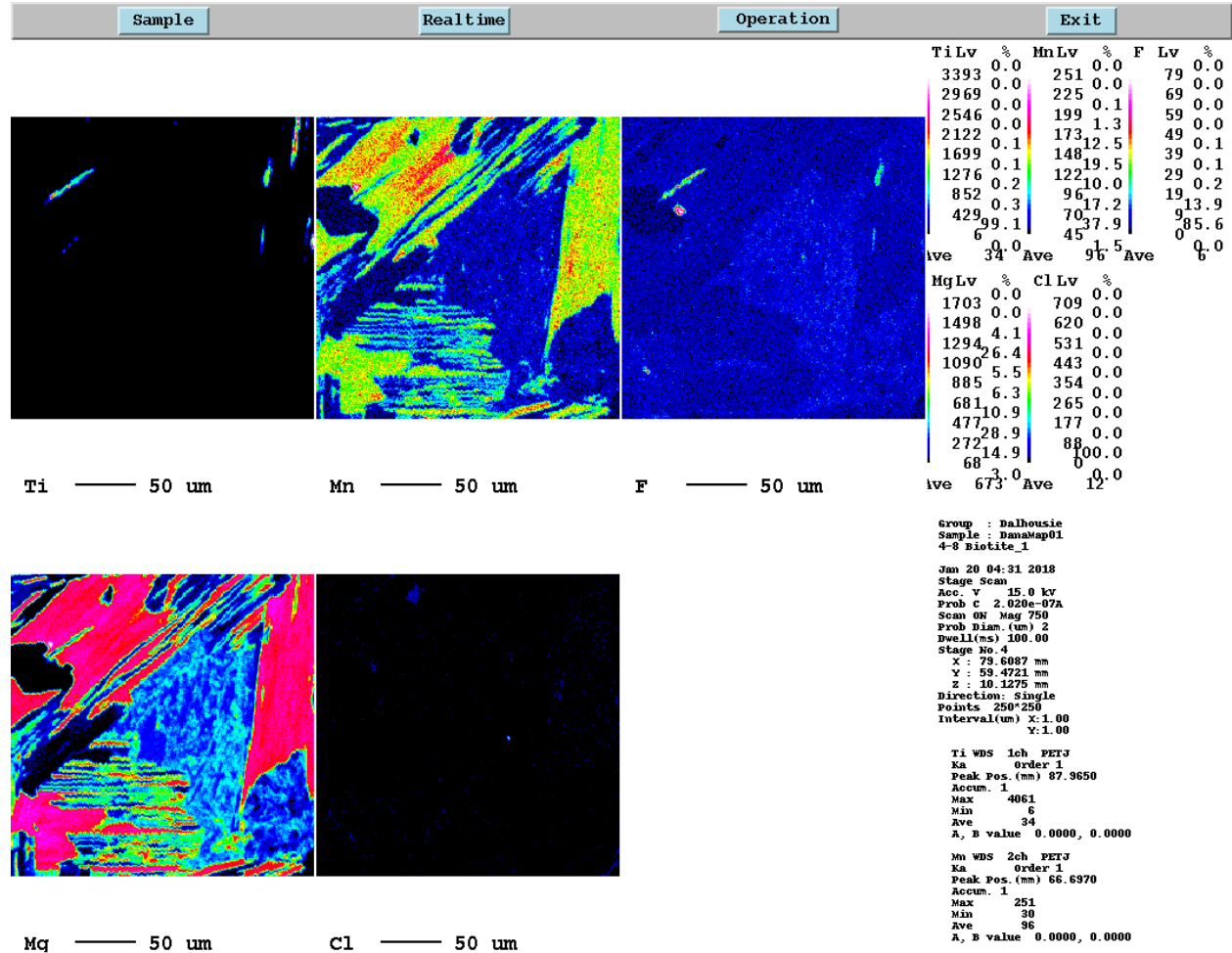Figure 1 – B1 – X-ray compositional map of thin section 4-8

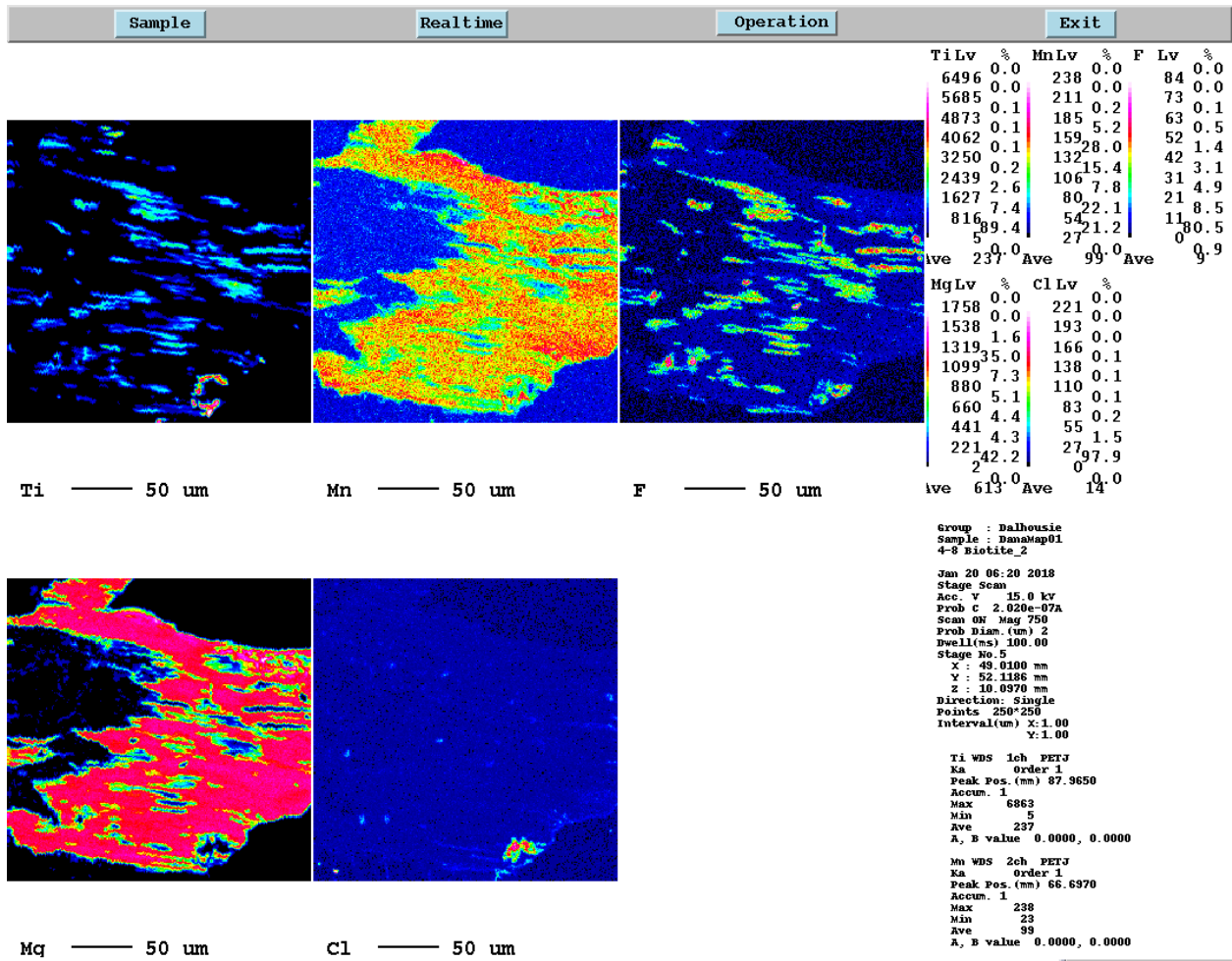Figure 2 – B2 – X-ray compositional map of thin section 4-8

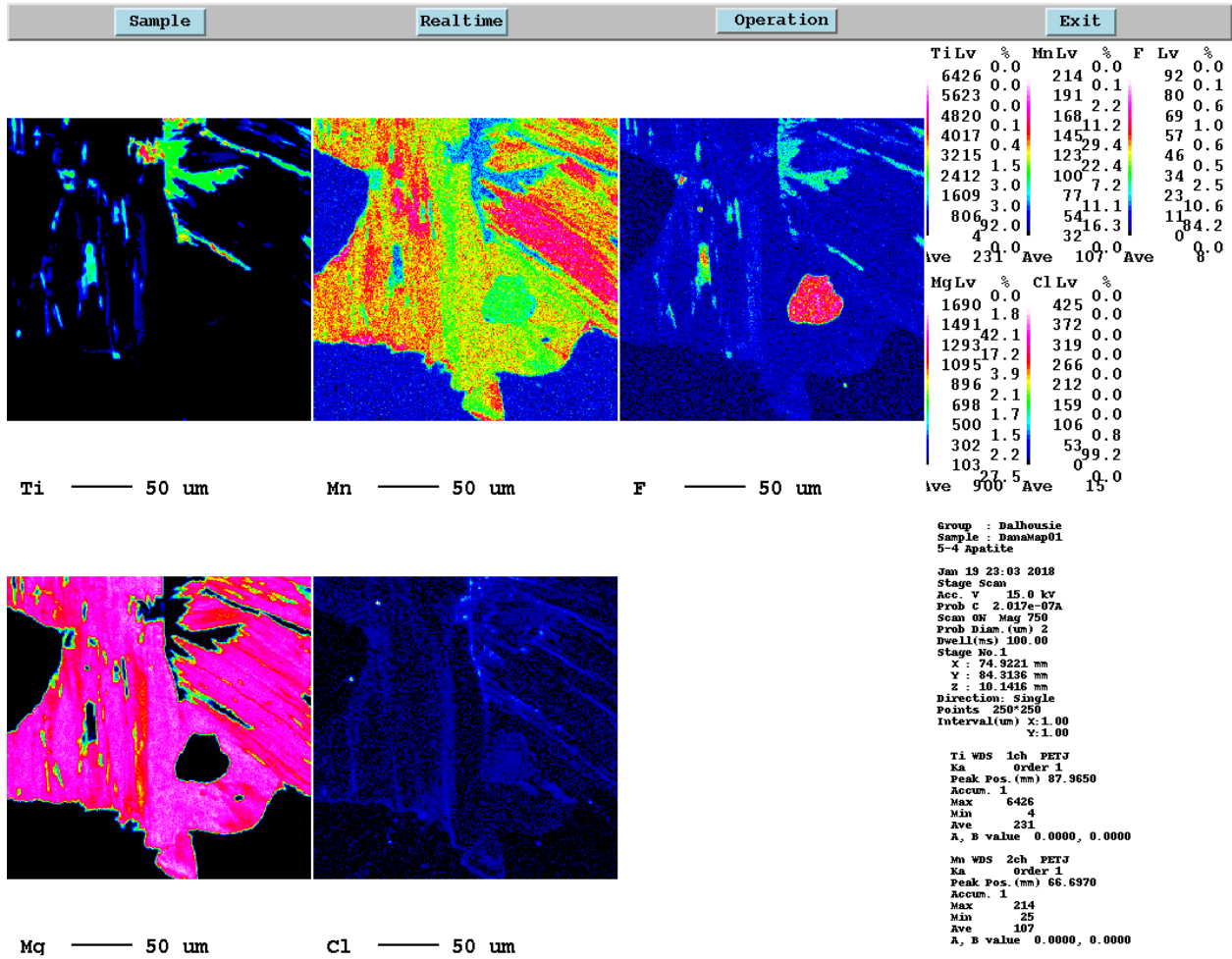Figure 3 – B3 – X-ray compositional map for thin section 5-4

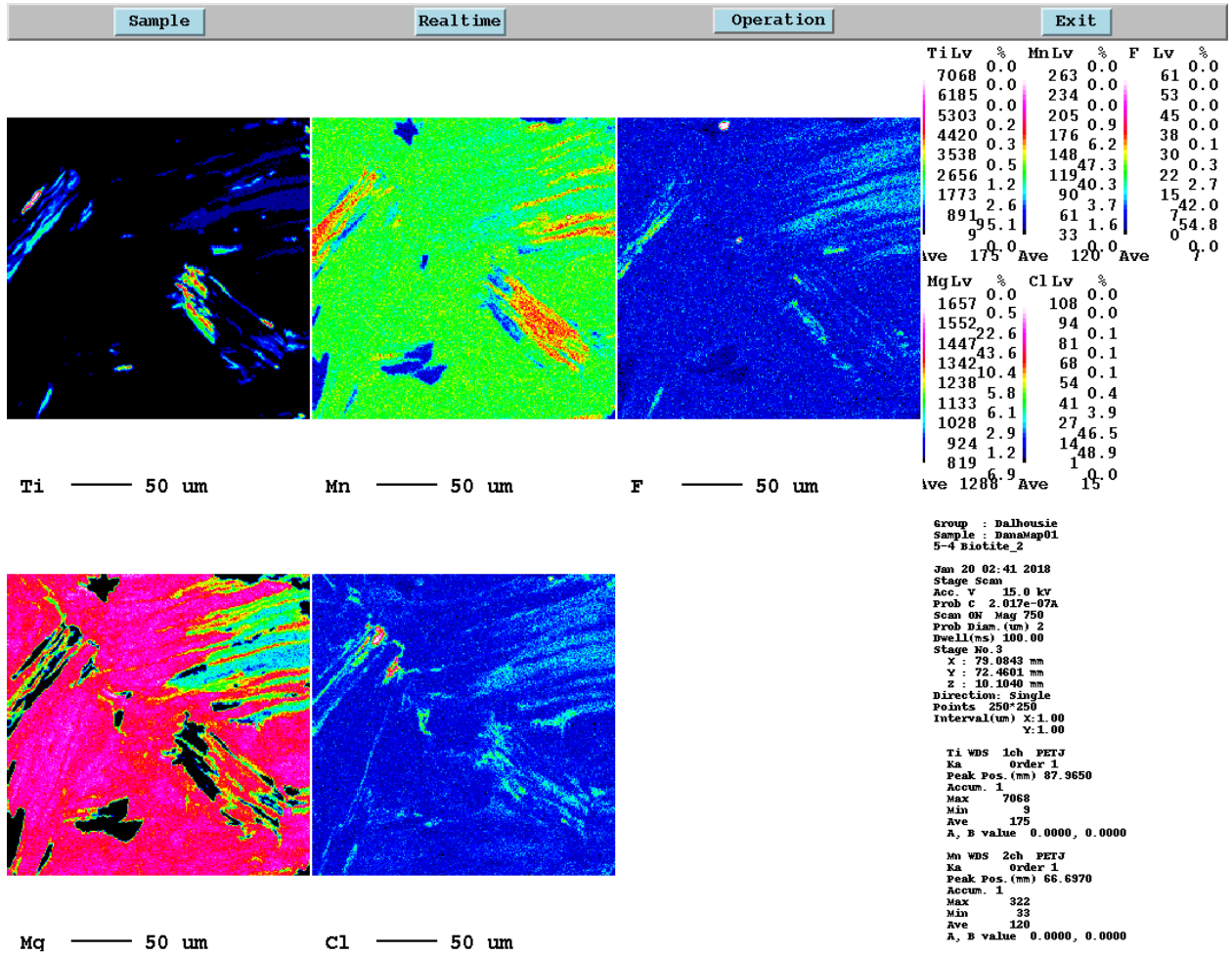Figure 4 – B4 – X-ray compositional map of thin section 5-4

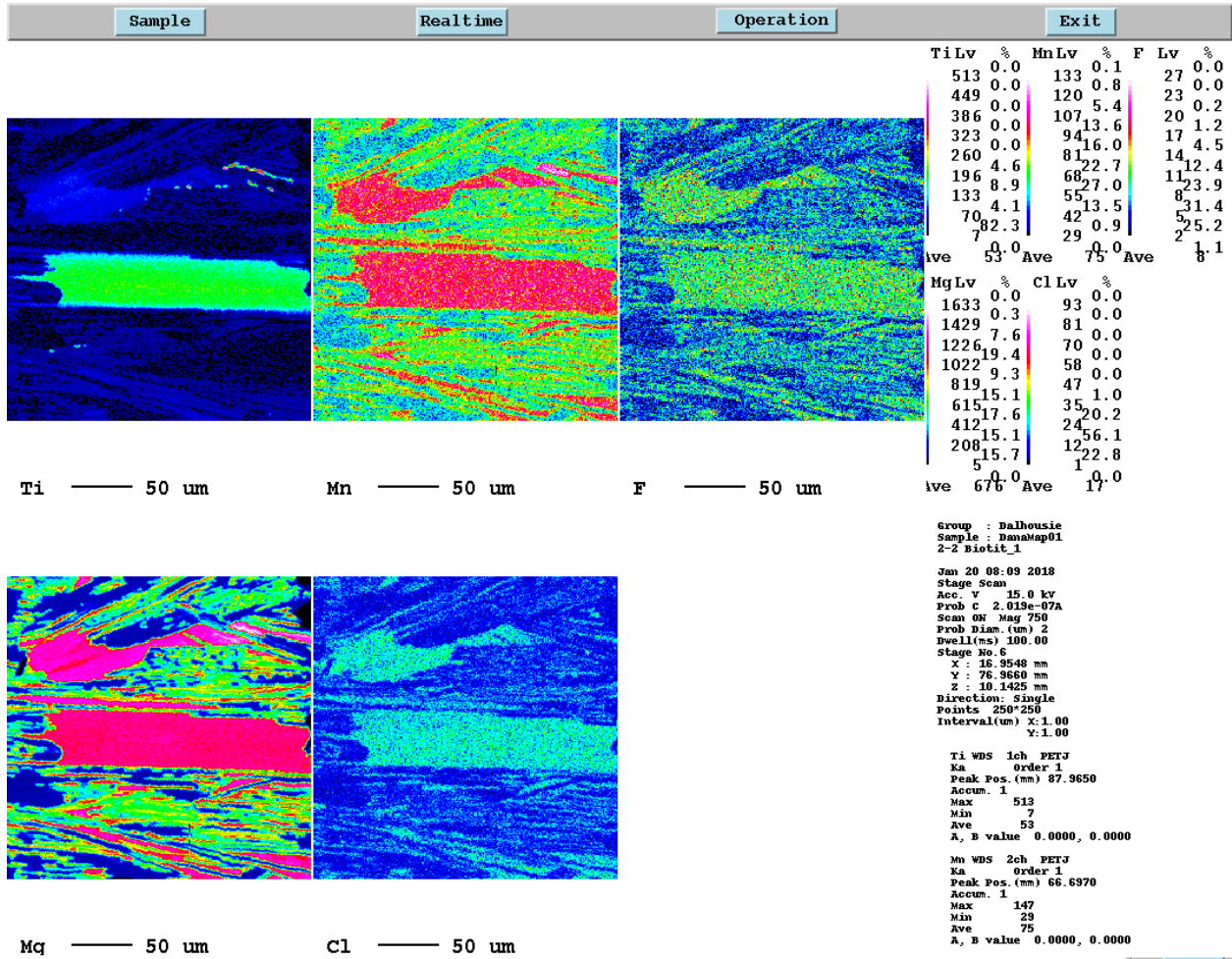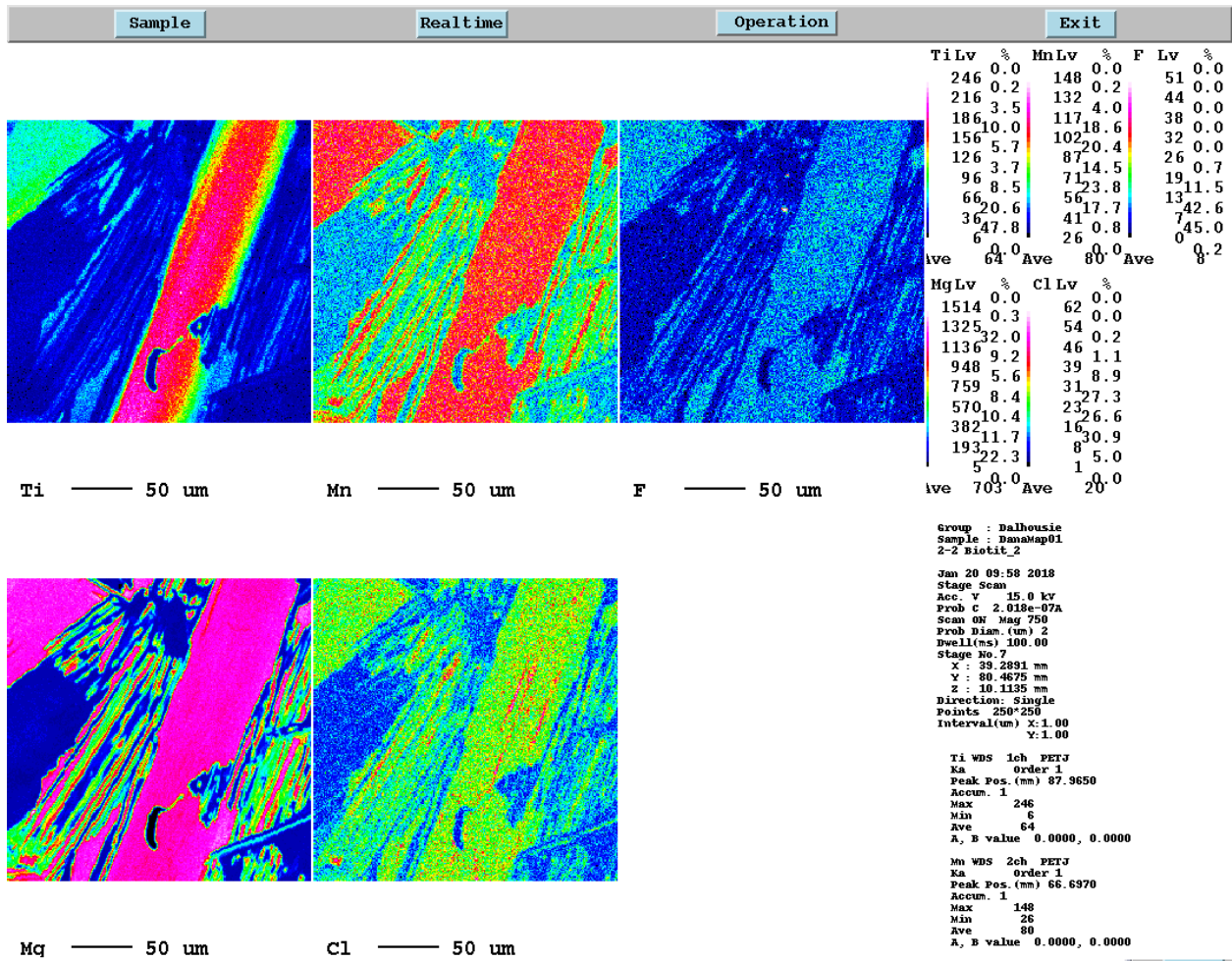Figure 5 – B5 – X-ray compositional map of thin section 2-2

Figure 6 – B6 – X-ray compositional map of thin section 2-2

Appendix C – EPMA and LA-ICP-MS Data

Table 1 – B1 – EPMA Major Oxide Data

Table 1 - B1

Sample No.	1DKTAll-4-4-1	1DKTB-4-3-1	1DKTM-4-3-1	1DKTT-4-3-2	2DKTL-3-2-2	3DKT7-3-1	3DKT2-4-1	3DKT1-4-1	3DKT2a-036-1	2DKT1-036-1
Location	Mixing Zone	Mixing Zone	Mixing Zone	Mixing Zone	Edge of Mixing Zone	Central Dyke	Central Dyke	Central Dyke	Prospect	Peggy's
No. of analyses	n = 10	n = 10	n = 10	n = 8	n = 10	n = 10	n = 10	n = 10	n = 10	n = 10
wt %	Ave. 2σ	Ave. 2σ	Ave. 2σ	Ave. 2σ	Ave. 2σ	Ave. 2σ	Ave. 2σ	Ave. 2σ	Ave. 2σ	Ave. 2σ
SiO_2	71.66 ± 3.94	72.87 ± 4.43	73.32 ± 8.94	74.93 ± 7.65	72.55 ± 4.30	71.59 ± 4.96	73.41 ± 5.24	72.49 ± 2.92	66.24 ± 4.30	70.62 ± 6.35
TiO_2	0.392 ± 0.11	0.433 ± 0.15	0.452 ± 0.14	0.38 ± 0.14	0.293 ± 0.19	0.527 ± 0.21	0.384 ± 0.10	0.458 ± 0.11	0.531 ± 0.27	0.537 ± 0.23
Al_2O_3	15.97 ± 1.86	15.66 ± 2.34	15.16 ± 4.58	14.80 ± 4.17	14.71 ± 2.27	16.09 ± 2.25	14.45 ± 2.64	15.79 ± 1.83	18.07 ± 2.84	16.36 ± 4.60
CaO	2.632 ± 0.34	2.403 ± 0.34	2.875 ± 0.74	1.979 ± 0.59	2.335 ± 0.40	1.926 ± 0.22	2.762 ± 0.60	2.216 ± 0.27	3.143 ± 0.66	2.201 ± 0.61
FeO	0.131 ± 1.23	0.129 ± 1.22	0.099 ± 1.51	0.094 ± 1.20	0.067 ± 0.71	0.084 ± 1.64	0.071 ± 0.93	0.077 ± 0.94	0.093 ± 0.83	0.095 ± 1.62
MnO	1.701 ± 0.05	1.821 ± 0.05	1.402 ± 0.60	1.486 ± 0.05	1.311 ± 0.03	1.948 ± 0.04	1.701 ± 0.04	2.189 ± 0.04	1.256 ± 0.04	1.266 ± 0.06
MgO	1.369 ± 0.54	1.155 ± 0.58	1.290 ± 0.70	1.048 ± 0.78	0.808 ± 0.66	1.569 ± 0.80	1.649 ± 0.56	1.281 ± 0.56	2.391 ± 0.55	1.262 ± 0.53
Na_2O	2.317 ± 0.32	2.165 ± 0.39	2.185 ± 0.71	2.144 ± 1.06	2.715 ± 0.42	2.399 ± 0.26	2.075 ± 0.41	2.275 ± 0.27	2.646 ± 0.35	2.455 ± 0.64
P_2O_5	2.723 ± 0.14	2.321 ± 0.24	2.456 ± 0.10	2.226 ± 0.17	4.538 ± 0.17	3.359 ± 0.10	2.437 ± 0.12	2.668 ± 0.06	4.939 ± 0.14	4.652 ± 0.24
K_2O	0.092 ± 0.22	0.090 ± 0.12	0.117 ± 0.18	0.148 ± 0.07	0.123 ± 0.14	0.124 ± 0.30	0.128 ± 0.16	0.138 ± 0.15	0.139 ± 0.38	0.203 ± 0.30
Total	98.99 ± 1.14	99.04 ± 0.54	99.36 ± 1.14	99.24 ± 1.39	99.45 ± 0.54	99.616 ± 0.56	99.067 ± 0.51	99.582 ± 0.33	99.448 ± 1.00	99.651 ± 0.59

*Standards used were: Kaersutite, Sanidine and Garnet

Table 2 – B2 – LA-ICP-MS Whole Rock Data

Table 2										
Sample Name	3DKT2-4-1	3DKT7-3-1	3DKT1-4-1	3DKT2a-036-1	2DKT1-036-1	1DKTAll-4-4-1	1DKTB-4-3-1	1DKTM-4-3-1	1DKTT-4-3-2	2DKTL-3-2-2
Location	Interior Dyke	Interior Dyke	Interior Dyke	Prospect	Peggy's Cove	Mixing Zone	Mixing Zone	Mixing Zone	Mixing Zone	Edge of Mix. Zone
REE (ppm)	Ave	Ave	Ave	Ave	Ave	Ave	Ave	Ave	Ave	Ave
La	15.08	13.85	19.57	25.78	22.32	17.82	12.95	16.25	19.90	10.24
Ce	26.15	23.61	33.09	46.48	40.38	33.72	25.06	31.28	35.74	20.51
Pr	3.21	2.84	3.97	5.74	5.04	3.71	2.83	3.57	4.00	2.36
Nd	14.96	12.79	17.54	26.51	23.08	15.81	12.35	15.34	16.84	10.25
Sm	3.35	2.80	3.76	6.22	5.95	3.73	2.86	3.52	3.62	2.63
Eu	0.62	0.69	0.54	1.13	0.93	0.50	0.55	0.45	0.32	0.65
Gd	2.96	2.53	3.19	5.31	4.90	3.07	2.47	2.87	2.99	2.42
Tb	0.41	0.32	0.42	0.65	0.63	0.44	0.35	0.41	0.41	0.37
Dy	2.69	2.07	2.71	3.98	4.17	2.89	2.29	2.74	2.60	2.40
Ho	0.44	0.35	0.47	0.63	0.71	0.48	0.40	0.50	0.43	0.41
Er	1.28	1.05	1.43	1.71	2.01	1.44	1.19	1.50	1.20	1.17
Tm	0.17	0.13	0.19	0.20	0.25	0.21	0.17	0.21	0.17	0.16
Yb	1.37	0.99	1.60	1.46	1.95	1.86	1.35	1.81	1.28	1.17
Lu	0.16	0.13	0.20	0.17	0.22	0.23	0.18	0.23	0.17	0.14
Sc	21.49	16.59	18.77	18.24	13.47	15.14	11.37	12.89	12.80	11.20
Y	12.61	9.91	13.41	17.11	20.19	12.53	10.45	13.12	11.45	11.69
Rb	182.70	182.00	227.50	180.60	123.33	204.80	131.60	163.53	129.00	184.40
Sr	210.40	166.10	142.63	211.00	134.73	167.10	128.47	151.50	127.93	99.67
Ba	580.67	226.10	252.60	989.33	543.33	299.63	165.97	214.50	163.93	313.23
Pb	2.86	8.28	1.66	17.52	8.80	5.55	8.58	4.91	2.06	12.77
As	0.49	1.66	1.05	1.05	0.46	0.76	0.87	0.66	0.46	2.27

Con't.	3DKT2-4-1	3DKT7-3-1	3DKT1-4-1	3DKT2a-036-1	2DKT1-036-1	1DKTAll-4-4-1	1DKTB-4-3-1	1DKTM-4-3-1	1DKTT-4-3-2	2DKTL-3-2-2
Zr	73.90	104.67	188.57	15.45	35.73	77.63	105.67	126.13	51.98	41.74
Hf	2.00	2.90	5.10	0.38	0.93	2.02	2.98	3.54	1.61	1.18
Nb	7.20	5.27	6.41	7.55	6.86	8.58	7.70	6.87	8.08	10.30
Ta	0.94	0.68	0.78	0.72	0.65	2.05	2.00	1.78	1.76	1.57
Ti	1851.33	1234.33	1487.33	1477.67	1342.00	2847.50	2669.00	2502.67	2221.00	1981.00
V	41.90	31.25	42.40	29.78	27.03	43.41	40.39	43.71	32.16	23.52
Ni	0.16	37.57	2.23	2.12	0.18	0.23	10.16	0.85	0.34	17.19
U	2.05	2.34	4.00	1.62	1.02	5.29	3.61	4.79	4.13	11.22
Th	5.31	6.72	7.80	8.04	4.96	8.06	5.09	5.84	6.20	4.16
Cr	23.28	60.73	47.50	14.89	15.54	22.52	37.77	27.78	17.46	24.02

*Standard used was NIST610 synthetic glass

Please refer to the electronic appendix for raw EPMA and LA-ICP-MS data.